UNIVERSITY OF HELSINKI REPORT SERIES IN PHYSICS

HU-P-D255

Voxel-level dosimetry of ^{177}Lu-octreotate: from phantoms to patients

Eero Hippeläinen

Department of Physics
Faculty of Science
University of Helsinki

HUS Medical Imaging Center
Department of Clinical Physiology
and Nuclear Medicine

Comprehensive Cancer Center
Helsinki University Central Hospital

Helsinki, Finland

ACADEMIC DISSERTATION

To be presented, with the permission of
the Faculty of Science of the University of Helsinki,
for public criticism in Auditorium of Department of physics, D101,
Gustaf Hällströmin katu 2, 00560, Helsinki,
on December 2nd, 2017, at 12 o'clock noon.

Helsinki, 2017

Supervisors:

Docent Mikko Tenhunen
Department of Radiation Oncology
HUCH Comprehensive Cancer Center
Helsinki
Finland

Docent Antti Sohlberg
Joint Authority for
Päijät-Häme Social and Health Care
Department of Clinical Physiology and
Nuclear Medicine
Finland

Pre-examiners:

Professor Katarina Sjögreen Gleisner
Department of Medical Radiation Physics
Lund University
Sweden

Docent Tommi Noponen
Department of Nuclear Medicine
Turku University Hospital
Finland

Opponent:

Professor Michael Ljungberg
Department of Medical Radiation Physics
Lund University
Sweden

Report Series in Physics HU-P-D255
ISSN 0356-0961
ISBN 978-951-51-2779-2 (printed version)
ISBN 978-951-51-2780-8 (pdf version)
http://www.ethesis.helsinki.fi

Unigrafia Oy
Helsinki 2017

E. Hippeläinen: Voxel-level dosimetry of 177Lu-octreotate: from phantoms to patients, University of Helsinki, 2017, 43 pages. University of Helsinki, Report Series in Physics, HU-P-D255

Keywords: Internal dosimetry, quantitative nuclear medicine imaging, radionuclide therapy

Abstract

In radionuclide therapy, the patient is injected with relatively high amounts of therapeutic radiopharmaceutical which localises to target tissue and emits ionising radiation. Unfortunately, a perfectly targeting radiopharmaceutical has not been discovered and part of the radiopharmaceutical accumulates to healthy tissues, which are also thus irradiated. In order to ensure safe use, the absorbed dose of radiation-sensitive organs must be monitored.

Internal radiation dosimetry in the field of medical physics is measurement, calculation and assessment of the absorbed dose from pharmaceuticals labelled with radionuclides. Typically, assessment is based on blood samples, external radiation probe measurements or imaging. The last ten years has been a time of rapid development in the field of nuclear medicine imaging. Hybrid imaging using single photon computed emission tomography (SPECT) combined with computed tomography (CT) enables the estimation of organ function and the following of the kinetics of radiopharmaceuticals, with high localisation precision. In addition to technical improvements, developments in image reconstruction algorithms have made quantitative SPECT/CT imaging possible. Combining recent advancements, the patient specific dosimetry of radionuclide therapies has become possible and is an interesting field of study in nuclear medicine.

The focus of this thesis is on patient specific dosimetry of ^{177}Lu labelled somatostatin analogue ^{177}Lu-DOTA-Tyr3-octreotate (^{177}Lu-DOTATATE) treatments and development of internal dosimetry software. ^{177}Lu-DOTATATE is a radiopharmaceutical that binds to somatostatin receptors and is used to treat patients with metastatic neuroendocrine tumours. Recent studies have shown significant treatment outcome improvements with ^{177}Lu-DOTATATE when compared to previously used somatostatin analogue treatments. However, the kidneys are the healthy organ which receives the highest amount of radiation dose from ^{177}Lu-DOTATATE treatments and could be the organ that limits the number of treatments a patient can tolerate. In addition, absorbed dose to kidneys varies highly from patient to patient and thus patient specific dosimetry is recommended. Despite many years of dosimetry research and the existence of several published scientific dosimetry tools, there is no clinically validated kidney dosimetry software for ^{177}Lu-DOTATATE treatments. The aim of this thesis was to study quantification accuracy of ^{177}Lu radionuclide using SPECT/CT imaging and to study

mean absorbed doses to kidneys and dose distribution characteristics of ^{177}Lu-DOTATATE. A streamlined voxel level absorbed dose software for clinical practice was developed and validated for kidney dosimetry of ^{177}Lu-DOTATATE treatments.

The effect of reconstruction methods on ^{177}Lu quantification accuracy was studied using an anthropomorphic phantom. The phantom was filled with known ^{177}Lu sources and scanned with patient imaging protocol using one SPECT/CT camera at Helsinki University Central Hospital (HUCH). Acquired data were reconstructed using different image compensation methods and results were compared with known source activities in the phantom. It was found that Monte Carlo simulation based scatter compensation and SPECT detector response compensation improved ^{177}Lu quantification accuracy considerably. Similar findings were also observed with data from patients treated with ^{177}Lu-DOTATATE.

A Monte Carlo simulation study using simplified kidney models and a realistic XCAT digital phantom was carried out to investigate absorbed dose distribution of ^{177}Lu. A fast absorbed dose calculation method (sMC) was also tested and later implemented into the developed dosimetry software. Two main findings were that electrons emitted by ^{177}Lu can be assumed to absorb locally when the resolution of the imaging system is taken into account and the photon cross-irradiation can contribute significantly to total absorbed dose especially in the vicinity of highly active volumes.

Using ^{177}Lu-DOTATATE patient data, two different kidney absorbed dose calculation methods were compared. Comparing the mean kidney absorbed dose with the estimated maximum absorbed dose, it was observed that ^{177}Lu-DOTATATE accumulates unevenly to kidney causing significantly heterogeneous dose distribution within kidneys. In addition, a simplified imaging protocol was found to be adequate for dosimetry purposes and was later adopted clinical practice.

Combining previous findings new voxel level dosimetry software was developed. The clinical feasibility of the proposed software was tested with digital phantom simulations and reanalysing patient data from ^{177}Lu-DOTATATE treatments. The software was found to be reliable and to speed up and simplify the dosimetry workflow.

Preface

This thesis project was carried out between 2010 and 2017 at various institutes. I would like to thank: The Department of Physics at the University of Helsinki and the Helsinki University Central Hospital Comprehensive Cancer Center. In particular I would like to thank HUS Medical Imaging Center and the staff of the Nuclear Medicine Department.

I am grateful to Professor Sauli Savolainen for introducing the world of dosimetry of internal emitters for me over a decade ago. I warmly acknowledge the head of the doctoral program of Materials Research and Nanosciences (MATRENA) Professor Jyrki Räisänen. Travel grants for doctoral candidates have made it possible to meet and learn from other researches around the world. Special thanks to Professor Kai Nordlund, Dr Flyura Djurabekova, Docent Antti Kuronen and the rest of the crew from material and particle simulation groups. I have always felt warmly welcome to Kumpula's acceleration laboratory and I am looking forward to joining the interesting morning coffee and Friday evening discussions.

I am especially grateful to my supervisors Docent Mikko Tenhunen and Docent Antti Sohlberg for their support, fruitful discussions and guidance through this exciting project. They have always found time for me and enlightened me in the fields of dosimetry and image reconstruction. I truly wish that we can continue to collaborate in the future too. I wish also to thank the other co-authors of the original articles, Hanna Mäenpää, Jorma Heikkonen and Vappu Reijonen.

I had the honour of having Professor Katarina Sjögreen Gleisner and Docent Tommi Noponen as the official reviewers of this thesis. I express my gratitude to their constructive and positive comments. I am also privileged to have Professor Michael Ljungberg as the opponent for the doctoral dissertation. I also wish to express my gratitude to Chris Constable for his friendship and help with the English language.

I also want to express my gratitude for the financial support to the Instrumentarium Science Foundation and to HERMES Medical Solutions. In addition, HUS Medical Imaging Center for the scientific award that helped me to finish this thesis.

I express my ineffable gratitude to adjunct professor and a skilful neurosurgeon Martin Lehecka and his neurological surgery team for *Craniotomia subtemporalis l. dx. et extirpation cavernomatis*. They did their best and made it possible for me to be here to enjoy this moment.

I also thank all of my medical physicist colleagues with whom I regularly enjoy daily lunch at 11 o'clock sharp, and share the latest rumours. Special thanks to the staff of the Nuclear Medicine Department at Meilahti and Jorvi hospitals and my dear colleagues: Outi, Toni and Miia.

I owe my deepest gratitude to my parents Maritta and Mikko Hippeläinen for all the freedom, trust, support and possibilities. Their hard work, stories and professional discussions about patient cases and research projects are still inspiring me. I also want to thank my brothers Pekka and Lauri for their time and refreshing lessons in the aerodynamics of flying plastic disks.

Finally, I wish to express my gratitude to the most important ones: my family. I want to thank my fiancée Annina Mara for all the love and patience during these year. Our two children, Aura and Unto, are wonderful and I am so proud to be father to them. I think we should start to plan our new adventure as soon as possible.

Käpylässä, Helsinki 7th of November 2017

List of original articles

This thesis consists of an introductory part followed by four original articles, which are referred to by the Roman numerals **I** - **IV** throughout the text.

I **Hippeläinen, E**, Tenhunen, M, Mäenpää, H, Sohlberg, A, Quantitative accuracy of Lu-177 SPECT reconstruction using different compensation methods: phantom and patient studies. *EJNMMI Research* 2016;6:16.

II **Hippeläinen, E**, Tenhunen, M, Sohlberg, A. Fast voxel-level dosimetry for Lu-177 labelled peptide treatments. *Physics in Medicine and Biology* 2015;60:17:6685-6700.

III Heikkonen, J, Mäenpää, H, **Hippeläinen, E**, Reijonen, V, Tenhunen, M. Effect of calculation method on kidney dosimetry in Lu-177-octreotate treatment. *Acta Oncologica* 2016;55:9-10:1069-1076.

IV **Hippeläinen, ET**, Tenhunen, MJ, Mäenpää, HO, Heikkonen, JJ, Sohlberg, AO. Dosimetry software Hermes Internal Radiation Dosimetry: from quantitative image reconstruction to voxel-level absorbed dose distribution. *Nuclear Medicine Communications* 2017;38:5:357-365.

Studies presented in this thesis had local research committee's approval (nr 51/12.12.2011).

Author's Contribution

Voxel dosimetry for ^{177}Lu-DOTATATE research project was mainly carried out by the author. Author's contribution to original articles included to this thesis is listed below.

Study I: The author planned and performed all the phantom measurements, cross-calibration, reconstructed and analysed phantom and patient data, and wrote the majority of the manuscript.

Study II: The author planned the cross-irradiation study, performed XCAT phantom and kidney model simulations and dose calculations. The manuscript was mainly written by the author. In addition, the author was also responsible for coding of the vxlPen main program for PENELOPE Monte-Carlo simulation package.

Study III: The author performed verification cross-calibration measurements and participated in discussion about the dosimetry methods at HUCH, Comprehensive Cancer Center. The author also commented upon the manuscript and participated in writing the dosimetry part of the paper.

Study IV: The author performed XCAT simulations and reconstructions, and absorbed dose calculations for the selected patient group using HIRD software. In addition, the author analysed the results and wrote the majority of the manuscript.

Symbols and abbreviations

3D	Three-dimensional
$\tilde{A}$	Total number of nuclear decays
AC	Attenuation correction
c	Detected counts
CDR	Collimator-detector response
C_{insert}	True activity concentration in the insert
cps	Counts per second
cRC	Concentration recovery coefficient
CT	Computed tomography
$CTDI_{vol}$	Computer tomography dose index
D	Absorbed dose
DCF	Dose conversion factor
DPK	Dose point kernel
FKD	Fast kidney dose method
GEP	Gastroenteropancreatic
HIRD	Hermes Internal Radiation Dosimetry
HU	Hounsfield unit
HUCH	Helsinki University Central Hospital
LAR	Long acting repeatable
MC	Monte Carlo
NET	Neuroendocrine tumour
NURBS	Non-uniform rational basis spline
OLINDA	Dosimetry software OLINDA/EXM
PET	Positron emission tomography
PRRT	Peptide receptor radionuclide therapy
PVE	Partial volume effect
R_{insert}	Count density within the insert
RR	Resolution recovery
S	Absorbed fraction
SC	Scatter correction
SI	Système International d'unités (International System of Units)
SPECT	Single photon emission computed tomography
SV	Small VOI
$\hat{S}_{vol}$	Calibration coefficient (cps/MBq)
$T_{1/2}$	Half-life
T_{eff}	Effective half-life
TAC	Time activity curve
TEW	Triple energy window
TIAC	Time integrated activity curve
TRT	Targeted radionuclide therapy
V_k	Kidney volume
VOI	Volume of interest
vxlPen	Customised main program for PENELOPE simulation code

WKV	Whole kidney volume
XCAT	Extended cardiac-torso digital phantom.
λ	Decay constant
v_T	Target voxel
v_S	Source voxel

Contents

1 Introduction

Neuroendocrine tumours (NETs) are relative rare (about 230 incidences per year in Finland [1]) neoplasms that can arise from different endocrine and nervous system cells. Interestingly, the incidence of NE Ts has been reported to be markedly increased in Canada [2], United States [3] and Europe [4], which partly reflects the increased availability of advanced radiological imaging and diagnostic methods. Gastroenteropancreatic NETs (GEP-NET) typically grow slowly and are observed as incidental findings during surgery, after extensive growth or when hormonal excretion of tumour causes clinical symptoms [3]. Patients with symptoms suggestive of NETs should be referred to a centre that is specialised in these diseases and histological and immunohistochemistry tests are mandatory to confirm the diagnosis [4]. Based on immunohistochemistry markers to reflect tumours proliferation activity (Ki67 and mitotic count), NET are classified into neuroendocrine tumour (G1 or G2) or into neuroendocrine carcinoma (G3) grades [5]. Symptoms and outcomes vary enormously among NET patients. Relative 5-year survival for pancreatic NETs varies from over 90% to less than 10%, depending on grade, stage and the site of origin of the tumour [6, 7].

Currently the only curative treatment for GEP-NETs is surgery. Unfortunately, over 80% of patients have metastases in spleen, liver or in both and thus pharmacological treatment and peptide receptor radionuclide therapy (PRRT) are the only options to suppress tumour growth and spread [3]. The standard treatment for NETs of any size is somatostatin analogues. Tumour response to the somatostatin treatment is generally considered to be poor, but disease stabilisation of 50%-60% has been reported [4].

Most of the GEP-NETs overexpress somatostatin receptor subtype 2 that can be targeted with radiolabelled pharmaceuticals. Promising clinical trial data has been published about PRRT using ^{177}Lu-[DOTA0,Tyr3]-octreotate (^{177}Lu-DOTATATE, Lutathera®, AAA) radiopharmaceutical [8-12]. This year a randomized clinical phase III trial investigating Lutathera®'s clinical efficacy reached its data cut-off date [13]. The study included 229 patients from 41 different sites with inoperable and somatostatin receptors expressing GEP-NETs. Patients were randomised into ^{177}Lu-DOTATATE treatment group (111 patients) and to a control group (110 patients). At the time of interim analysis, the median progression free time had not been reached in the ^{177}Lu-DOTATATE treatment group while it was 8.4 months in the control group treated with conventional high-dose octreotide long-acting repeatable (LAR) somatostatin analogue. For the ^{177}Lu-DOTATATE group, progression free time was estimated to be 40 months.

In PRRT, a radiolabelled peptide is typically introduced to a patient by an intravenous infusion. The radiopharmaceutical is distributed within the patient by perfusion and partly accumulated to tumour cells. The free radiopharmaceutical is secreted or metabolised by kidneys and liver, respectively. This pharmacokinetic process is characterised by the pharmaceutical properties and organ functions of the patient, but the biological effect of treatment is mostly based on radiation emitted by the radionuclide. The major drawback of radionuclide therapy is that healthy tissue also receives damage from ionising radiation

and thus dosing should be personalised to avoid possible healthy tissue complications. Conventional dosing methods rely on an amount of injected activity scaled by weight or body surface area, but these methods fail to take into account the pharmacokinetics or radiation characteristics of the radionuclide. Fortunately, radionuclides used in PRRT are typically selected so that they emit, in addition to locally ionising radiation (β^- or α particles), also x-rays or γ radiation, which can be localised and quantified with a gamma camera. Ideally, the radiation exposure from the radiopharmaceutical, measured as absorbed dose, can then be estimated from the images. Image based dosimetry is not a novel concept and has been investigated as long as there have been imaging methods available. However, within the last ten years developments in reconstruction algorithms and the increasing availability of computing power have made quantitative imaging and image based dosimetry possible in daily practice. It should be noted that current image based dosimetry methods are based mostly on post-therapeutic imaging and there is no method available that could predict the outcome of the radionuclide therapy.

In this study, dosimetry methods for radionuclide therapy are investigated. Because of the current clinical interest, this thesis focuses on image based dosimetry of ^{177}Lu-DOTATATE treatments. Despite the long history of dosimetry studies and recent promising clinical results, the availability of clinical dosimetry software for radionuclide therapy is poor and methods are badly standardised. Therefore, topics presented in this thesis have demand in clinical practice and are scientifically interesting especially within the field of medical physics.

1.1 Why do dosimetry?

The most important motivation for radionuclide dosimetry is to predict response and toxicity of the treatment. The evidence base for the use of internal dosimetry in clinical practice is reviewed by *Stigari et al.* [14]. The review included 92 radiotherapy dosimetry and dose-effect correlation studies found in PubMed. Even though the selected studies were rated to moderate or low clinical relevance categories, the evidence implies a correlation between delivered absorbed dose and the response and toxicity. Therefore, *Stigari et al*. concluded that dosimetry-based personalised treatments would improve outcome and increase survival.

Probably due to the high complexity and uncertainty of internal emitter dosimetry only few studies report dose-responses. With a blood sample –based method (not based on imaging) it has been found that absorbed dose to the red marrow predicts haematological toxicity better than the amount of injected activity of ^{131}I labelled antibody [15]. In another study, fast clearance of ^{166}Ho-1,4,7,10-tetraazacyclododecane-1,4,7,10-tetramethylene-phosphonic acid via kidney was found to induce renal toxicity with estimated kidney doses of 2.6-14 Gy [16]. In a recent study, nephrotoxicity after ^{177}Lu-DOTATATE treatment was found to be low, the mean absorbed dose to kidney being 20.1 ± 4.9 Gy [17]. Tumour dose-responses have been reported only in two PRRT studies. In a subset of 13 patients treated with ^{90}Y-[DOTA]-D-Phe1-Tyr3-octreotide (^{90}Y-DOTATOC, OctreoTher) Pauwels *et al.* found a significant correlation between estimated

dose to the tumour and the tumour size reduction [18]. The tumour dose estimates were based on quantitative ^{86}Y-DOTATOC PET scans and the mean dose was 232 or 37 Gy for responding or non-responding tumours, respectively. In an other study, Ilan et al. found a similar tumour-response from ^{177}Lu-DOTATATE treated patients [19]. The tumour response was estimated at the time the largest tumour reduction was observed. They used SPECT/CT images to quantify the activity in the tumours and thus only tumours larger than 2.2 cm were included in the study and the doses to tumour ranged from 20 to 340 Gy.

2 SPECT-based dosimetry of ^{177}Lu-DOTATATE treatments

2.1 Dosimetry workflow

A generalised workflow of image based dosimetry in targeted radionuclide therapy (TRT) is shown in Figure *2-1*. Briefly the process is as follows. A treatment radiopharmaceutical is introduced to a patient by an injection or infusion. Because the radiopharmaceutical is distributed heterogeneously within body by perfusion and kinetics of the radiopharmaceutical, kinetics of the radionuclide should be resolved temporally to get estimates of absorbed dose. This dynamic process can be followed, for example, by a series of single photon emission computed tomography (SPECT) acquisitions combined with computed tomography (CT). Based on the quantitative SPECT image reconstructions, the dose distribution can be estimated using dose calculation methods.

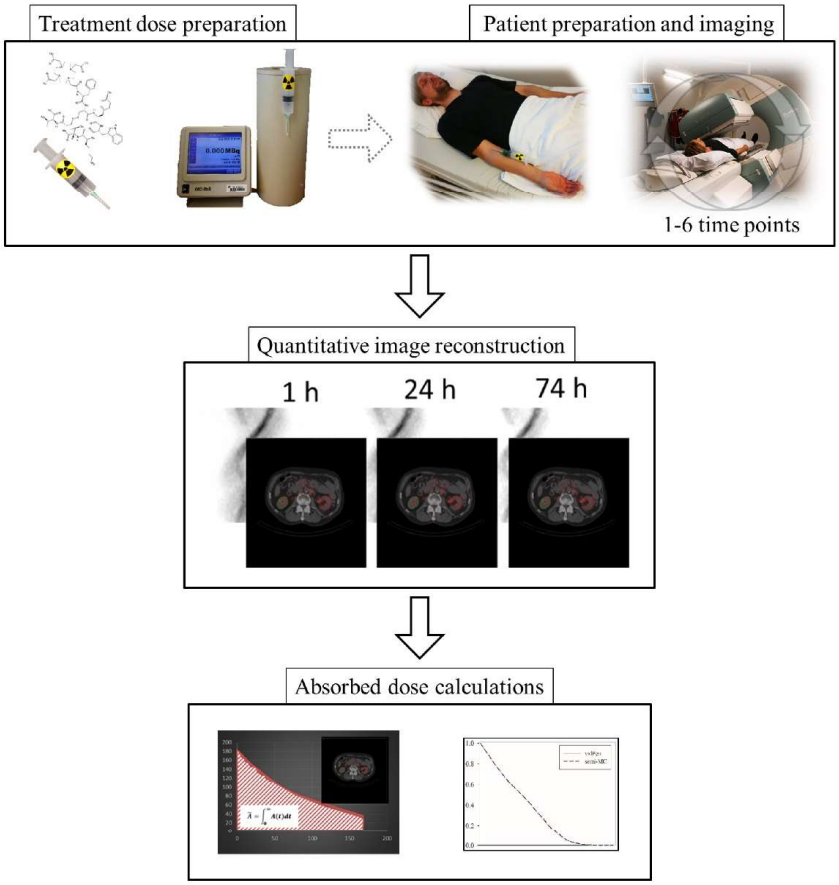

Figure 2-1. Example of radionuclide therapy dosimetry workflow.

To be able to quantify and follow the activity in patients, radionuclides used in TRT are typically selected so that they emit, in addition to non-penetrating radiation (β^- or α particles) also x-rays or gamma radiation (γ), which can be detected outside the patient without interventions [20]. The patient is imaged using a gamma camera that produces projections from the activity distribution.

Most of the activity quantification for dosimetry has been done using planar whole body scans. Although planar imaging method is relative fast and can easily cover the whole body, it lacks depth information and thus cannot separate overlapping organs from each other. In recent years, developments in image reconstruction compensation methods, hybrid SPECT/CT imaging systems and available computation power have made SPECT possible for daily practice [21, 22]. Combining SPECT imaging with CT, the 3D activity distribution can be measured and localised from the patient with a spatial resolution of approximately 1 cm or better.

Because the radiopharmaceutical distribution changes over time in the patient, the activity distribution is assessed using serial quantitative SPECT/CT scans. Ideally, the whole patient would be scanned continuously to cover radiopharmaceutical's kinetics in whole, but absorption, metabolism and excretion can take days and thus continuously repeated whole-body acquisitions with SPECT are not practically feasible. The sufficient number of SPECT/CT scans required for reliable sampling of time-activity curves (TACs) depends on the kinetics of the radiopharmaceutical. For example in the case of the ^{177}Lu-DOTATATE treatments, three or four acquisition time points have been shown to be clinically adequate for TAC measurements, starting from 1 hour and ending at around 168 hours or later after the treatment injection [23].

For dosimetry purposes, the total number of radioactive decays is of interest, because it is proportional to the emitted energy by the radionuclide. The total number of decays within a volume equals the area under the TAC, which can be solved by integration and is referred as time integrated activity curve (TIAC) or cumulated activity. Mostly because of practical reasons, the true TAC is sparsely sampled and thus integration of TAC is done numerically or analytically with the help of model fitting. Depending on the dosimetry method, TIACs are solved at the organ level or as in study **IV**, the TIACs are calculated for each image volume element (voxel) separately.

The aim of dosimetry is to obtain absorbed dose estimates from the target or critical organs. For that, the calculated TIAC values should be transformed into absorbed dose distributions. Probably the most widely used software for this is the OLINDA/EXM (OLINDA) that computes absorbed doses in standardised anatomic geometries (anthropomorphic digital phantoms) using pre-calculated conversion factors and organ average TIACs [24]. OLINDA was originally developed for risk assessment of internalised radionuclides and its use for patient specific dosimetry has been criticised [25, 26].

Heterogeneity of activity distribution can be taken into account by carrying out dose calculation using smaller volume elements instead of the organ averages. One obvious idea is to do dose calculations at the voxel level. There are numerous ways to do this, but mostly voxel level dose calculation methods can be categorised into the following three method types. The first and easiest absorbed dose calculation method is to assume that all the relevant radiation is absorbed locally and thus the total number of decays (TIAC) to dose conversion is just a multiplication with a dose conversion factor (DCF). The conversion method is simple to implement and fast to perform, but it does not take into account the cross-irradiation between voxels. The second calculation method is based on dose point kernels (DPK) that represent absorbed dose distribution as a function of distance from a point source. The TIAC image can be transformed to a dose distribution by convolving the image with a DPK. This method is also relatively fast, but needs special software to carry out the convolution. Other disadvantages are that DPK is voxel size-dependent and it should be pre-calculated for all materials separately in the investigated volume. Because the DPK method is restricted to one material, it cannot take into account tissue inhomogeneity and artefacts can occur at the boundaries of different tissue densities. The third method is Monte Carlo (MC) simulation that is considered to be the most accurate method available. In MC simulations, numerous random particle tracks are simulated utilising detailed interaction libraries for the radiation type and tissue in question. There are several different MC simulation packages available. However, none has wide clinical acceptance for radionuclide dosimetry, because simulations are time consuming, dependent on many parameters and cumbersome to set up.

In one part of this study, a hybrid dose calculation method that combines DCF and MC calculation methods is investigated for radionuclide therapy dosimetry. In the case of ^{177}Lu, mostly DCF method or OLINDA software has been used and both have their advantages and disadvantages. As mentioned earlier, the DCF does not take cross-irradiation into account and could lead to dose underestimations due to gamma radiation yield from ^{177}Lu. With OLINDA, absorbed dose estimates are based on organ averages, standardised geometries and homogeneous distributions and thus it cannot offer patient specific dose estimates.

2.2 Lutetium-177

Lutetium-177 (^{177}Lu) is an unstable radioisotope of the 71st element in the periodic table, lutetium. Because of its relatively short half-life (6.6 d), it is not naturally abundant and for medical use, it is produced in nuclear reactors irradiating ^{176}Lu or ytterbium-176 (^{176}Yb) with neutrons:

$$^{176}Lu(n,\gamma)^{177}Lu \quad (1)$$

or

$$^{176}Yb(n,\gamma)^{177}Yb\ \beta^{-}{}^{177}Lu, \quad (2)$$

respectively. All ^{177}Lu used in this study was produced by Advanced Accelerator

Applications (AAA, Saint-Genis-Pouilly, France) through the direct method (Eq. 1). The direct method yields an end product with ^{176}Lu, ^{177}Lu and a small amount of long lived ^{177m}Lu isotope. However, the portion of ^{177m}Lu has been reported to be less than 0.05% of the total activity and the contribution to absorbed dose calculations is negligible [27]. On the other hand, the indirect method (Eq. 2) requires complicated radiochemical separation process, but yields high specific activity and high radionuclide purity [28].

^{177}Lu disintegrates by β^- decay to the ground state and to three different excitation levels of hafnium-177 (^{177}Hf), the maximum released energy being 498.3 keV [29]. In Figure 2-2, the decay scheme of ^{177}Lu radionuclide with the main decays paths are shown. In addition to β^- particles, the decay process produces small amounts of x-rays, Auger and conversion electrons. The de-excitation of ^{177}Hf emits several gamma rays (γ) with different energy. The gamma transitions of 113 keV and 208 keV being the most abundant, emitting 6.2 and 10.38 photons per 100 decays, respectively. These gamma energies are important for image based dosimetry and diagnostic imaging, because they are intensive enough for imaging and the energies are suitable for detection with a gamma camera. On the other hand, the emitted β^- particles are therapeutically effective, having a short mean range of 0.7 mm in soft tissue. The β^- particles deliver energy to relatively small volumes, therefore sparing the healthy tissues surrounding tumours, but beta energies are high enough to deliver relatively homogeneous absorbed dose at cellular level [30].

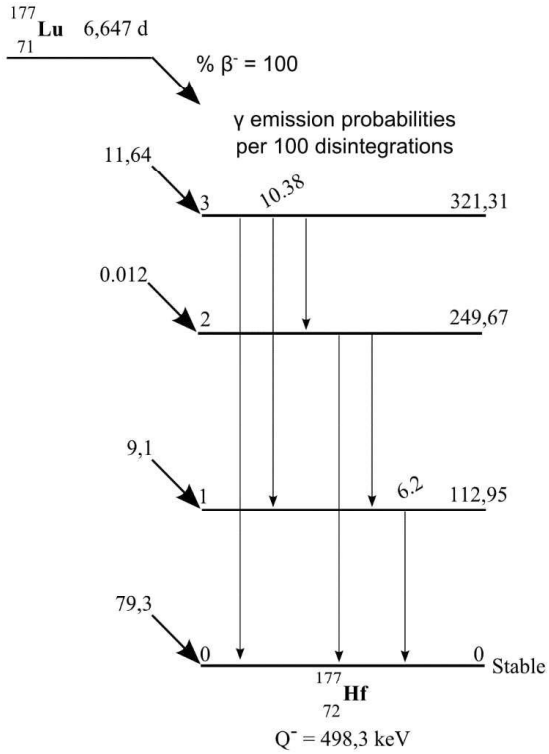

Figure 2-2. Simplified β^- decay scheme of ^{177}Lu radionuclide. Gamma emission probabilities of two transitions ($\gamma_{3,1}$ and $\gamma_{1,0}$), used for scintillation imaging, are shown. The decay scheme is based on data from Laboratoire National Henri Becquerel, available at www.nucleide.org [31].

2.3 ^{177}Lu-octreotate (^{177}Lu-DOTATATE)

In this thesis, experiments focus on dosimetry of ^{177}Lu-[DOTA0,Tyr3]-octreotate (^{177}Lu-DOTATATE, Lutathera®, AAA) radiopharmaceutical. Octreotate is one of many somatostatin analogues used in nuclear medicine [32]. The radiolabelled complex of octreotate,^{177}Lu-DOTATATE, has shown to bind to somatostatin receptor expressing tissues [33], especially it has a high affinity to somatostatin subtype 2 receptors [34]. In general, ^{177}Lu-DOTATATE treatment is well tolerated and has low and acceptable toxicity profile [12, 17, 35]. The first ^{177}Lu-DOTATATE experimental treatments on humans were carried out over ten years ago [11], but after that, numerous clinical experiments have been published.

2.4 Available internal dosimetry software

There are several dosimetry packages published for radionuclide therapy, which will be briefly reviewed here. As mentioned earlier, OLINDA/EXM is the most widely used dosimetry software available, although it was originally intended for radiation safety calculations rather than clinical internal radiation dosimetry per se [24]. OLINDA/EXM is based on pre-calculated radiation absorbed fractions (S) for the ten whole-body phantoms representing reference adults, children, and pregnant women. OLINDA/EXM has a multi-exponential fitting and integration subprogram (EXM) for organ average accumulated activity calculations, but no image reconstruction or VOI analysis tools. There are at least two separate programs, SPRIND [36] and ULMDOS [37], which provide the missing data analysis tools for OLINDA/EXM. Because the dose calculation is based on fixed S factors, individual variations in organ shapes and positions cannot be taken into account. OLINDA/EXM allows the user to scale absorbed doses for patient-specific organ masses, but the scaling affects only the self-irradiation dose component. A comparison study between OLINDA/EXM and full Monte Carlo dosimetry method using patient specific geometry (CT data) found a difference of 26% in mean organ doses for simulated ^{131}I radionuclide distributions, even when the organ mass correction was applied in OLINDA/EXM calculations [38]. For tumour dose estimations, OLINDA/EXM uses spherical models which are treated as completely isolated objects and cross-irradiation dose is completely neglected.

In addition to OLINDA/EXM, several research groups have published their own dosimetry packages. The most recent one is called Lundadose [39], which provides versatile absorbed dose calculation and analysis tools for SPECT and planar data. A good overview of other available software is given in a paper by *Grimes et al.* [40], where they also present JADA dosimetry software. Gamma camera vendors and healthcare companies have also published commercially available dosimetry software (Table 2-1). These software packages have typically limited functionalities and are tied to company's analysis software and thus they cannot handle other vendors' imaging data.

Table 2-1. *Commercially available dosimetry software for radionuclide therapies.*

Name of the software software	Company name	Features
Dosimetry toolkit	GE Healthcare	Quantitative reconstruction and resident time calculations for OLINDA
DOSEFX	Comecer	TAC analysis, fitting and dose calculations
Simplicit^{90}Y	Mirada in co-operation with BTG	For ^{90}Y SIRT therapy, CE mark certificated
Stratos	Philips Healthcare	Full dosimetry package, research use only. Also voxel level calculations
Automated Internal Dosimetry Research Tool	Siemens Healthineers	Full ^{177}Lu specific dosimetry package, research use only

3 Aims of the study

The aim of this thesis was to develop and validate patient specific dosimetry software for radionuclide therapies, focusing on neuroendocrine tumour treatments with ^{177}Lu-DOTATATE. Studies were designed to cover all the main steps of radionuclide therapy dosimetry, namely: quantification, kinetic analysis and dose calculations. In addition, the developed dosimetry workflow and software was compared to OLINDA/EXM.

Studies in this thesis were designed to:

I Evaluate the effect of SPECT reconstruction compensation methods to quantification accuracy of the ^{177}Lu radionuclide

II Study absorbed dose characteristics of ^{177}Lu in tissue and validate fast absorbed dose calculation method for the dosimetry software

III Compare the small volume method and the mean kidney dose calculation method with each other

IV Study feasibility of the voxel level kidney dosimetry and validate the dosimetry software.

4 Materials and methods

In the following section, basic dosimetry quantities and used methods are introduced. The content of the section follows the same logical progression as the original articles.

4.1 SPECT based quantification of ^{177}Lu

The aim of quantification is to exactly quantify the concentration of radioactivity within a given volume in absolute units, for example kBq/cm^3. Unfortunately, the SPECT imaging process is compromised by photon attenuation, photon scatter, and the detector system's relatively poor resolution (partial volume effect, PVE), and thus SPECT is not inherently quantitative. These image deteriorating effects can be partly compensated during properly optimised iterative image reconstruction and images proportional to the amount of activity can be produced. More comprehensive reviews of compensation methods are published, for example, by Ritt et al. [22].

For radionuclide therapy dosimetry, the activity quantification is essential, because activity is proportional to dose rate at a given time point. In this study, we only considered the SPECT/CT methods for quantifying ^{177}Lu activity distributions, but it should be noted that planar imaging has also been frequently used. However, it has been shown in simulation and patient studies that a solely planar imaging method is prone to overlap and attenuation correction problems and the TAC estimate accuracy is worse than with a SPECT protocol [41, 42]. The blood activity ^{177}Lu levels can also be measured from blood samples as it is done in bone marrow dosimetry [43], but that method was not used in this thesis.

4.1.1 SPECT imaging protocol

SPECT acquisition of ^{177}Lu distribution within patients and phantoms were carried out using a two headed Siemens Symbia T2 gamma camera (Siemens Healthineers, Erlangen, Germany) combined with a two slice CT. The SPECT imaging protocol was the following. One field of view SPECT scans were acquired in noncircular step and shoot mode, to produce 64 projection of the source. The time per projection was 20 s and it took approximately 15 minutes to complete the scan. The projections were acquired into 128 x 128 matrix producing the pixel size of 4.79 mm at the detector plane. The higher 208 keV photon peak was acquired using 20% width energy window (range: 187.3 – 228.8 keV) associated with an upper (228.8 – 270.4) and a lower (145.6 – 187.2 keV) scatter energy windows. Medium energy general purpose collimators (MEGP) were used to optimize camera sensitivity and decrease the collimator septal penetration.

The ^{177}Lu SPECT imaging protocol used in this thesis was similar to other protocols reported in the literature [44-46] and was generally consistent with the guidelines of European Association of Nuclear Medicine (EANM) and Committee on Medical Internal Radiation Dose (MIRD) [47].

4.1.2 SPECT image reconstruction

Two implementations of an ordered subset expectation maximisation (OSEM) algorithm [48], Flash3D (Siemens, Germany, Erlangen) [49] and HybridRecon (HERMES Medical Solutions, Stockholm, Sweden) [50] were used for SPECT image reconstructions. The latter was further implemented for the new dosimetry software (study **IV)**. Both reconstruction software packages provide compensations for photon attenuation (AC) [51], photon scatter (SC) and resolution recovery (RR, also known as collimator-detector response CDR) [52]. The fundamental difference between the implementations lies in the scatter correction. In Flash3D, a triple energy window (TEW) scatter compensation method is used, where the scatter portion from the detected primary photons is estimated using a weighted ratio of photons detected in the upper and lower energy windows [53, 54]. On the other hand, HybridRecon does scatter estimations based on fast MC simulations in a density map derived from patient's CT image and the measured activity distribution [55]. The number of iterations and subsets varied between studies and are shown in Table 4-2. In Flash3D a post-reconstruction Gaussian filter of 8.4 mm full width at half maximum (FWHM) was also applied. PVE correction other than CDR were not used in any study. All images were reconstructed into isotropic (4.79×4.79×4.79 mm^3) voxels in 128×128×128 matrix.

Table 4-2. *SPECT image reconstruction parameters in different studies.*

Study	OSEM Algorithm	Iterations	Subsets	Post-filtering
I	HybridRecon	15	16	-
II	HybridRecon	15	8	-
III	Flash3D	8	4	8.4mm FWHM Gaussian
IV	HybridRecon	8	16	-
	Flash3D	8	4	8.4mm FWHM Gaussian

Image reconstruction produces images that represent the distribution of activity averaged over the acquisition. The intensity in voxels is, with some limitations, proportional to activity and is usually represented in unit of counts (c) or counts per second (cps), if normalised by the projection acquisition time.

4.1.3 CT imaging protocol and reconstruction

SPECT acquisition was always followed by a CT scan that covered SPECT's field of view. The scan time of CT was about 37 seconds with the tube voltage of 130 kV. Automated Exposure Control and dose modulation options of CARE Dose 4D (Siemens Healthineers, Germany, Erlangen) were used with the quality reference tube current-time product of 85 mAs. A mean volume CT dose index ($CTDI_{vol}$) was 10.8 mGy. The CT data was reconstructed to 512 × 512 matrix producing axial pixel size of 0.98 × 0.98 mm and 3.0 mm slice thickness.

The CT images were reconstructed at acquisition workstations using two different reconstruction kernels. A sharp (B35) kernel image was used for localisation and kidney VOI delineation. For the attenuation map, another reconstruction was done using a smoother kernel (B08s) and the CT voxel values presented in Hounsfield units (HU) were converted to linear attenuation coefficients using a bilinear conversion equation [51]. The attenuation map was further used during the SPECT reconstruction for photon attenuation and scatter compensations.

4.1.4 Cross-calibration of imaging system

To be able to quantify activities from reconstructed SPECT images, the system sensitivity and the relation to the absolute activity should be resolved. Cross-calibration between the SPECT/CT imaging system and the dose calibrator can be done using a calibration phantom filled uniformly with a known amount of ^{177}Lu activity (Figure 4-3). The phantom is scanned with the SPECT/CT system and reconstructed. A calibration coefficient ($\hat{S}_{vol}$ in cps/MBq), that is the ratio of reconstructed counts in the active source and the total activity in the phantom, can then be determined from the phantom image. With the $\hat{S}_{vol}$ coefficient, the reconstructed SPECT image voxel values can be converted into activity concentrations (in MBq/cm^3) by simple multiplication.

In studies presented in this thesis, two different calibration phantoms were used to obtain the $\hat{S}_{vol}$. The phantom 1 was a 0.5 litre bottle with 234.6 MBq of ^{177}Lu activity submerged in a water filled Jaszczak phantom (Studies **I** and **IV**). The phantom 2 was a modified Alderson radiation therapy phantom with a source cylinder insert (radius = 3.3 cm, height = 8.0 cm and activity = 53 MBq) in abdomen area (Studies **III** and **IV**). The cross-calibration method is in line with the available guidelines [45, 47]. In addition, the stability of $\hat{S}_{vol}$ was followed with the phantom 2, after ^{177}Lu-DOTATATE treatments were begun at the HUCH. The SPECT/CT system was found to be stable (unpublished quality assurance data). Similar calibration method have also been shown to be reproducible in a multicentre study [56].

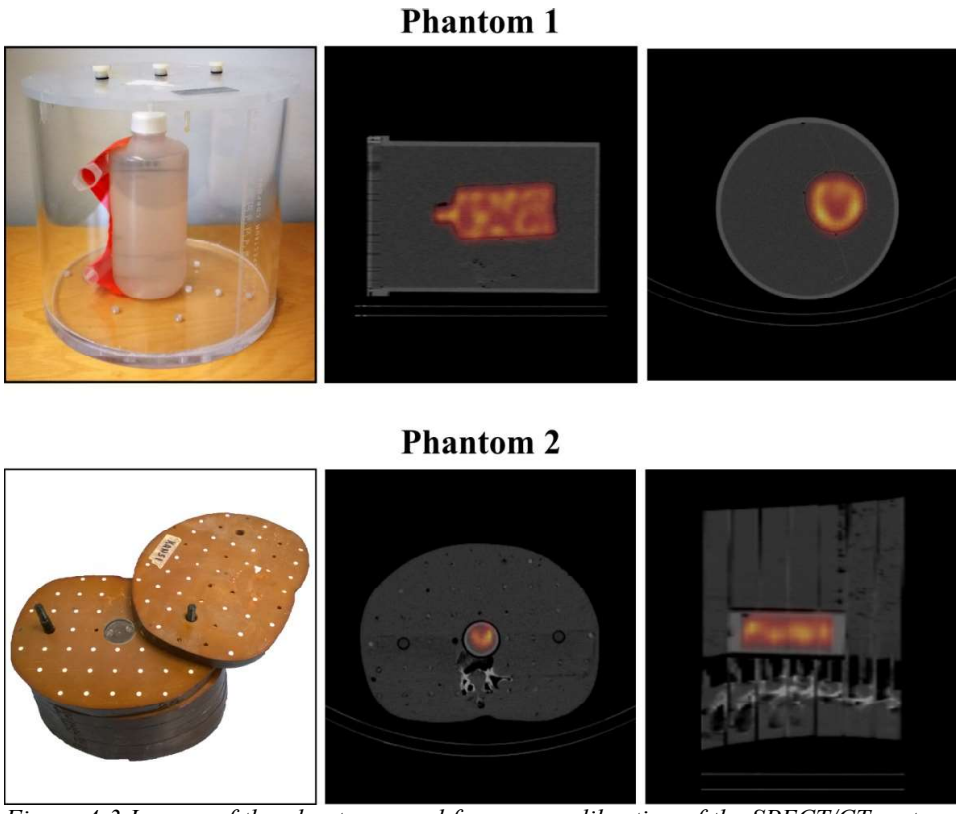

Figure 4-3 Images of the phantoms used for cross-calibration of the SPECT/CT system. (Top row) A Jaszczak phantom with a ^{177}Lu filled plastic bottle insert and (bottom row) an anthropomorphic phantom including a ^{177}Lu filled cylindrical container. In the middle and right columns, transversal and coronal SPECT images overlaid with CT images are also shown from both phantoms.

4.1.5 Dose calibrator activity measurements

All activity inserted in the phantoms or infused to patients were measured using a dose calibrator (Atomlab 500, Biodex, New York, USA). The calibrator's performance was followed daily by ^{57}Co constancy test, biannually by linearity measurements using a ^{99m}Tc source and annually by accuracy measurements using ^{133}Ba source. In addition, the dose calibrator's performance was verified using a standard reference source of ^{177}Lu (Polatom, Otwock, Poland).

4.1.6 Quantification accuracy of ^{177}Lu using SPECT/CT

In study **I**, the effect of reconstruction compensation methods to quantification accuracy of ^{177}Lu was investigated. This study was conducted using a modified anthropomorphic

thorax phantom with nine spherical inserts. Six of the inserts were part of the NEMA image quality phantom with volumes ranging from 0.4 to 26.1 ml and three were in-house made with volumes of 30.3, 30.3 and 104.4 ml. The inserts were filled with ^{177}Lu solution and placed into the phantom with background activity. From reconstructed images, a concentration recovery coefficient (cRC) was calculated for each insert

$$cRC = \frac{1}{C_{insert}} \cdot \frac{R_{insert}}{V_{insert}\hat{S}_{vol}}, \quad 4.3$$

where R_{insert} is the count density within the VOI, V_{insert} is the true volume of the VOI, $\hat{S}_{vol}$ is the system calibration factor and the C_{insert} is the true concentration in the insert. VOIs were drawn on the CT image based on physical boundaries of the inserts and then transferred to the corresponding SPECT image.

The study also included patient SPECT/CT data from ten ^{177}Lu-DOTATATE treatments (see Table *4-3*). The data were acquired at three time points at 24 , 74 and 168 h post-treatment. Anatomical kidney VOIs were delineated based on CT images at each time point and the activity in the kidneys were estimated from SPECT images for each time point. A mono-exponential function ($y(t) = Ae^{-\lambda t}$) was fitted to kidney time-activity series for TAC estimation. The effective half-life ($T_{eff} = \frac{ln2}{\lambda}$) and absorbed dose to the kidneys were estimated separately for each patient and each reconstruction separately.

4.2 Absorbed dose

The basic physical quantity to study ionisation radiation effects on biological tissue is the absorbed dose, *D*. The absorbed dose is defined as the mean energy imparted, $d\bar{\varepsilon}$, into a volume of tissue with the mass, dm, that is

$$D = \frac{d\bar{\varepsilon}}{dm}. \quad (4)$$

The unit of measure for absorbed dose is Jkg^{-1} in base units and in International System of Units it is known as grey (Gy). By taking into account the target-source relationship and radiation nuclide characteristics, equation (4) can be extended for internal emitters at the voxel level as follows. The absorbed dose to target voxel v_T due to radioactivity located in source voxel v_S is expressed as

$$D\left(v_T \leftarrow v_S\right) = \check{A}(v_S) \sum_i \frac{n_i E_i \varphi_i\left(v_T \leftarrow v_S\right)}{m_T}, \quad (5)$$

where $\check{A}(v_S)$ is total number of nuclear decays in the source voxel v_S, E_i and n_i are the energy and frequency of each radiation type *i*, the fraction of absorbed energy $\varphi_i\left(v_T \leftarrow v_S\right)$ from the source to the target from the each radiation type and m_T is the

mass of the target voxel. Equation (5) is known as the MIRD formalism [57], which contains the essentials of internal dose calculations. Equation (5) can be separated into two parts: i) $\tilde{A}(v_S) = \text{TIAC}$ that depends on the kinetics of the activity and ii) $\sum_i \frac{n_i E_i \varphi_i(v_T \leftarrow v_S)}{m_T} = S(v_T \leftarrow v_S)$ that depends on the physical properties of media, geometry and decaying radionuclide. The latter is also known as the *absorbed fraction*.

4.2.1 Voxel based absorbed dose calculations of ^{177}Lu

In mean organ dosimetry calculations (OLINDA type software), the S factor for β particles is typically considered to be 1 for self-irradiation case $S(v_T \leftarrow v_T)$, and zero for cross-irradiation $S(v_T \leftarrow v_S)$. This is due to the fact that the ranges of β particles used in TRT are relative short compared to organ sizes and their distances from each other, thus the cross-irradiation is considered negligible. In case of ^{177}Lu, the contribution of photon cross-irradiation dose to total dose is also considered to be within a few percentages and typically omitted from the absorbed dose calculations [23]. However, when carrying out voxel level dosimetry calculations, voxel sizes and therefore also distances are at the ranges from millimetres to centimetres and thus S factor for cross-irradiation could be notably larger than zero.

In study **II**, the radiation characteristics of ^{177}Lu and relevance of cross-irradiation dose in voxel level dosimetry is investigated. In addition, a semi-MC absorbed dose calculation method (sMC) for ^{177}Lu is introduced. The sMC assumes that electrons are absorbed locally (DCF method) and photons are modelled using an accelerated MC-simulation method based on delta-scattering [58]. The idea is to omit computationally troublesome electron simulations, but still include potentially important components of photon dose to the dose calculations. The photon interactions are simulated using cross-section tables defined by Berger et al. [59] and all materials are assumed to be water with varying density based on the density map (converted CT image). Simulations of photons are traced until their energy drops below E_{abs} = 15 keV, after which they are assumed to be absorbed in their current voxel. All the secondary particles produced by photons are assumed to be locally absorbed. In study **II**, sMC method is also compared to a full Monte Carlo dose method (vxlPen) and validity of sMC assumptions are tested.

In study **II**, cross-irradiation dose was studied using a simple digital kidney phantom. An ellipsoidal kidney model (axis sizes of x = y = 7 cm and z = 12 cm) filled with a homogeneous ^{177}Lu activity was simulated in a homogeneous soft tissue media. The kidney to background activity concentration ratio varied from 1:1 to 20:1 between the simulations. The photon cross-irradiation dose between background and the kidney was studied by comparing absorbed dose calculations with and without photon simulations in the kidney model. In the second part of the study, the amount of cross-irradiation to an identical target kidney volume was recorded at nine different distances from the surface of the active kidney.

The comparison between a full MC dosimetry implementation vxlPen and sMC was

carried out using a digital XCAT phantom [60]. XCAT is a detailed whole-body digital phantom based on non-uniform rational basis spline (NURBS) defined anatomy. XCAT was simulated with default male settings and average organ activities measured from ten randomly selected ^{177}Lu-DOTATATE treated patients used in study **I**. The phantom was forward projected to produce SPECT data using in-house MC based projector [61]. From the projections, twenty noise realisations were created and reconstructed using HybridRecon. From the images, the absorbed doses calculations were done using vxlPen and sMC and the differences of 3D dose distribution were evaluated.

4.3 ^{177}Lu-DOTATATE treatment protocol at Comprehensive Cancer Center

In the Helsinki University Central Hospital (HUCH) Comprehensive Cancer Center, patients are typically treated with four cycles of ^{177}Lu-DOTATATE infusion at eight-week intervals. Patients receive a kidney-protective amino acid infusion (Vamin 14 g N/I®) that starts half an hour before the treatment infusion and is continued up to eight hours. The treatment infusion takes 30 minutes to complete. Before and between treatment cycles, possible radiotoxicity (haematocixity) and renal toxicity unrelated to PRRT is followed with blood samples. Patients are released from the hospital one day after the treatment. The decision in order to proceed with follow-up treatments is made after the completion of four treatment cycles if the mean kidney absorbed dose does not reach 27 Gy.

Typical administered activity per treatment is 7.4 GBq of ^{177}Lu, which sums up to the total activity of 29.6 GBq from four treatments. The activity was lowered 75% or 50% for patients who had any signs of bone marrow toxicity. Other reasons for lower treatment activity were older age, previous chemotherapy, diabetes, hypertension, fragility and any combination of these.

The HUCH's treatment protocol follows the same pattern as reported in several publications and is in line with practical guidelines [62], a long amino acid infusion being an exception. Commonly, up to four hour infusion is reported [23, 63-65]. Reasoning for the longer amino acid infusion protocol is the observation in Sandström et al. article [43], that the activity in blood decreases fast within the first day and thus amino acid infusion was prolonged as long as practically feasible. Amino acid infusion causes nausea, but it can be treated and in general infusions have been well tolerated.

4.3.1 Patient data

Twenty-four consecutive patients with metastatic NETs (WHO grade G1 or G2) treated with ^{177}Lu-DOTATATE were included in the study. All the treatments were conducted in the Department of Radiotherapy, Comprehensive Cancer Center, HUCH, from February 2011 to August 2013. All patients had four treatment cycles. From the entire patient sample, smaller subgroups were selected for studies **I** and **IV** and the whole data were analysed in study **III**. The characteristics of patient data for each study and sampling criteria are shown in Table *4-3*.

Table 4-3. Number of patients and analysed treatments in studies **I**, **III** *and* **IV**. *The mean infused activities and patient selection criteria are also listed.*

Study	Number of patients in the study	Analysed treatments per patient	Mean infused activity (Range) GBq	Selection criteria
I	10*	1	6.8 (3.7 – 8.1)	Randomly from study **III**
III	24	4	7.1 (3.3 – 8.79)	Consecutive 177Lu-DOTATATE treatments from February 2011 to August 2013
IV	6*	2	4.3 (3.7 – 6.2) 7.7 (6.0 – 8.3)	Patients with reduced and normal treatment activities from study **III**

*Subgroup of study **III** patients

4.3.2 Dosimetry protocol in HUCH

Imaging for kidney dosimetry was carried out using SPECT/CT at 24, 72 and 168 hour after the treatment infusion. Some of the patients had also 1 hour post-treatment imaging time point, but it was not used for dosimetry. From the reconstructed images, the activity within both kidneys was measured using two different VOI-analysis method (see below). A mono-exponential or bi-exponential function was fitted to time-activity data and absorbed doses to both kidneys were calculated using a reference adult (female or male) phantom in OLINDA [24] software. The absorbed dose was scaled by the mass of kidney that was estimated from delineated volume.

4.3.3 Mean kidney dose

Mean absorbed dose to kidney was estimated delineating whole left and right kidney volumes (WKVs) from each of the three CT images separately. Delineation was based on observed physical boundary of the organ. The mean activity at certain time point was measured from corresponding calibrated SPECT images using the VOIs. Mono-exponential TAC fits and the mean absorbed doses were calculated using OLINDA/EXM for both kidneys separately.

4.3.4 Small VOI method

Approximation of maximum absorbed dose was measured using a spherical VOI with volume of 4 cm^3. The small VOI (SV) was positioned on the maximum activity region of the lateral kidney cortex and medulla on the three SPECTs at different time points. Mean activity within SVs were scaled to correspond the whole kidney volume. Scaled activities

were used to calculate mean estimated maximum absorbed dose to kidneys using OLINDA software.

4.3.5 Effect of activity sampling method to kidney dosimetry

In study **III**, the differences between WKV and SV activity sampling methods were studied. Rationale for comparison was that the both methods, WKV and SV, are used in published studies and the comparison gives insights of heterogeneity of ^{177}Lu-DOTATATE uptake in kidneys. Twenty-four consecutive patients with four treatment cycles were analysed using both methods and estimated absorbed doses and effective half-times (T_{eff}) were compared.

In addition, a less demanding imaging protocol for dosimetry was introduced. The fast kidney dose (FKD) method is based on conversion coefficient (k) determined from absorbed doses from the patients, effective half-life ($T_{½,eff}$) determined by mono-exponential fit to 24 and 168 h acquisition data and patient specific kidney volumes (V_k). The mean absorbed dose to kidney in FKD method was calculated using following equations:

$$D(Gy) = k * T_{½} * C_{24}/V_k \quad (6)$$

and

$$T_{½} = \ln(2) * 144 * \left[ln\frac{C_{24}}{C_{168}}\right]^{-1}, \quad (7)$$

where k = 0.021 mGy/g/MBq·s is a conversion coefficient, $T_{½}$ is the effective half-life (in hours) estimated from the observed kidney counts in the SPECT images C_{24} and C_{168} at 24 and 168 h acquisition time points, respectively and V_k is the mass of the delineated kidney volume assuming density being 1.00 g/cm^3. The FKD method was also compared to WKV and SV methods in study **III**.

4.4 Voxel level absorbed dose calculation method: HIRD

As a part of this thesis, a voxel level dosimetry software called HERMES internal radiation dose (HIRD) was developed. Software was developed in collaboration with HERMES Medical Solutions (Stockholm, Sweden) and HUCH Comprehensive Cancer Center. Software was developed to run under HERMES patient database application Gold (HERMES, Stockholm, Sweden). Next, the essential parts of voxel level dosimetry methods implemented in HIRD are presented, but auxiliary functionalities such as image co-registration algorithms, delineation tools and motion correction methods are outside the scope of this thesis.

The HIRD was developed to include all the necessary post-processing step of acquired data to perform voxel-level dosimetry for radionuclide therapies. In this study, ^{177}Lu radionuclide and ^{177}Lu-DOTATATE treatment data are employed because of their clinical importance.

4.4.1 Voxel level dosimetry workflow

The workflow of the HIRD software is shown in Figure *4-4*. In practice, the workflow is briefly as follows. The software is launched with input of all the necessary SPECT/CT datasets for dose calculation. At the first step, reconstruction parameters are chosen and the SPECT projection data are visualized for possible motion during imaging. Then, co-registration of SPECT and CT data is verified by the user and reconstruction is carried out for each SPECT/CT datasets separately. If misalignment between SPECT and CT data is noticed, it should be corrected to prevent attenuation and scatter correction artefacts. The correction can be done manually or using mutual information based automatic co-registration algorithm. After the reconstructions, CT images from different time points are registered to a reference CT image space. The registration can again be done manually or with help of automatic rigid co-registration algorithm. After satisfactory registration between time points is achieved, same transformations are applied to the SPECT data.

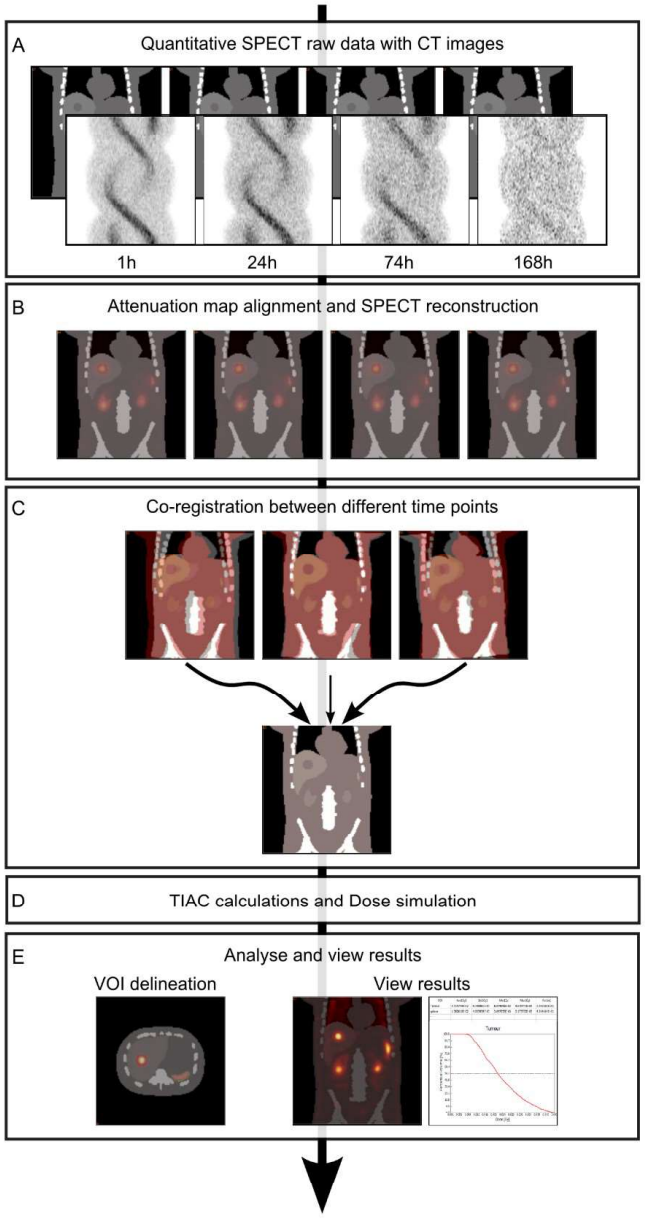

Figure 4-4. Dosimetry workflow implemented in HIRD. The workflow is as follows: A) Program is initiated with series of SPECT/CT datasets. B) Quality verification of SPECT data and alignment with CT data, motion correction, and reconstruction. C) Co-registration of CT images between different time points to same reference space. D) TAC fitting and integration voxel by voxel. E) Result overview, visualisation and saving.

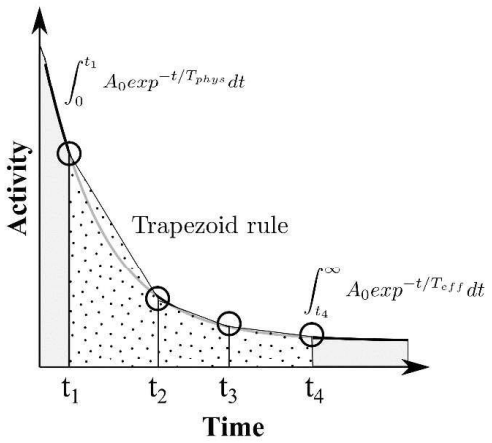

Figure 4-5 Example TAC and illustration of TIAC calculation method implemented within HIRD. Black circles represent SPECT/CT acquisition time points. Area under the curve is divided into grey and polka dot shaded depending on whether the integral is defined analytically or numerically using trapezoid rule, respectively. T_{phys} is half-life of the radionuclide and T_{eff} is effective half-life analytically estimated from the last two time points.

At this point, all SPECT and CT images should be aligned in the same reference space (that is, corresponding SPECT voxels at each time point represent the same volumes) and TAC analysis can be done. TAC analysis and integration is done in two different ways depending on how many SPECT/CT data sets the software is launched with. If HIRD is launched with more than one dataset, TAC and TIAC are estimated in three parts. The first part of TAC is extrapolated backwards, from the first acquisition time point to the treatment infusion, using a mono-exponential function with the physical half-life of the radionuclide (T_{phys}). The tail of the TAC curve is extrapolated with an exponential function with an effective half-life (T_{eff}) calculated from last two acquisition time points. Due to noise in voxel level TACs, T_{eff} is constrained to be equal or smaller than T_{phys}. Then, TIAC is calculated analytically at extrapolation parts and using the trapezoidal rule between acquisition points (Figure *4-5*). If only one dataset is used as input, TAC is modelled only using a mono-exponential function with the T_{phys} of used radionuclide. All the TAC estimates and TIAC calculations are done for each voxel separately. After TIACs are calculated, absorbed dose calculations are done using sMC method that was earlier introduced in study **II**.

The workflow of HIRD ends at the step where the user can view, analyse and save calculated voxel level absorbed dose distribution with realigned SPECT/CT data and delineated VOIs.

4.4.2 Testing HIRD and clinical utility

In study **IV**, the validity of voxel level dose calculation and clinical utility of the HIRD software for kidney dosimetry were tested. A digital XCAT phantom with a model of 50 ml liver tumour was created to simulate ^{177}Lu activity distributions in a ^{177}Lu-DOTATATE treated patient at 1, 24, 74, and 168 h post-treatment. Kinetics of ^{177}Lu-DOTATATE was modelled using a mono-exponential function, the parameters of which were averaged from ten randomly selected patients. SPECT projection data were simulated from the XCAT phantom using an in-house developed projector [61]. The density map of the XCAT phantom was converted to a CT image using inverted bi-linear conversion from HU units to density. From simulated SPECT/CT datasets photon and electron absorbed doses at the voxel level were separately calculated using HIRD. Mean absorbed dose to spleen, kidneys and to a liver tumour produced by electrons were compared to the analytically calculated reference organ doses ($D_{\text{ref,electron}}$). For $D_{\text{ref,electron}}$ calculation, photon contribution was neglected so that $D_{\text{ref,electron}}$ was equal to the sum of kinetic energy of electrons emitted by ^{177}Lu. $D_{\text{ref,electron}}$ was calculates as follows:

$$D_{ref,electron} = \frac{2.14 \times 10^{-11}}{(ln(2)/T_{eff})} \cdot A_0, \quad (8)$$

where T_{eff} is effective half-life of the organ, A_0 is activity in voxels at that organ at time of injection and 2.14×10^{-11} mGy / MBq is activity to absorbed dose conversion coefficient derived from the electron spectrum emitted by ^{177}Lu.

The HIRD workflow was also tested using clinical patient data. A subgroup of six patients with high and low activity ^{177}Lu-DOTATATE treatments were selected from the study **III** patient sample. Patients were re-analysed using the HIRD software and mean absorbed kidney doses were compared to OLINDA/EXM doses calculated earlier in study **III**.

5 Results

5.1 Quantification accuracy of ^{177}Lu

In study **I**, calibration of the SPECT/CT system was successfully carried out using the calibration phantom 1. Quantification accuracy of ^{177}Lu radionuclide using SPECT/CT imaging was measured using cRC (Equation 4.3) and results are summarised in Table 5-4. Recovery curves for all three studied methods are shown in Figure *5-6*. The quantification accuracy improves as more compensation methods are used and the most accurate results were achieved using AC-SC-CDR compensation methods. It should be noted that full activity recovery (cRC = 1) for any insert could not be achieved, which can partly be explained with partial volume effect. The inserts were delineated according to the physical boundaries from CT image and due to poorer resolution of SPECT some activity spills out from delineated volume. Another notable point is that including MC-simulation based SC method improved quantification accuracy especially for smaller sources.

Table 5-4. *Summary of quantification accuracy results of study* **I**. *Q1-Q9 are the inserts inside an anthropomorphic phantom.*

Insert label	**Q9**	**Q8**	**Q7**	**Q6**	**Q5**	**Q4**	**Q3**	**Q2**	**Q1**
Volume (cm^3)	0.4	1.2	2.6	5.5	10.8	26.1	30.3	30.3	104.4
Diameter (cm)	0.9	1.3	1.7	2.2	2.7	3.7	3.9	3.9	5.8
Activity (MBq)	0.52	1.24	2.69	5.80	11.90	27.16	30.43	31.15	105.18
	Measured activity (MBq)								
AC	0.05	0.17	0.60	1.73	4.78	14.18	13.78	14.72	66.24
AC-CDR	0.09	0.42	1.38	3.05	7.02	18.23	21.04	19.77	85.44
AC-SC-CDR	0.16	0.60	1.89	4.08	8.97	23.16	25.90	23.35	89.88
	cRC								
AC	0.10	0.13	0.22	0.30	0.40	0.52	0.45	0.47	0.63
AC-CDR	0.18	0.34	0.51	0.53	0.59	0.67	0.69	0.63	0.81
AC-SC-CDR	0.30	0.49	0.70	0.70	0.75	0.85	0.85	0.75	0.85

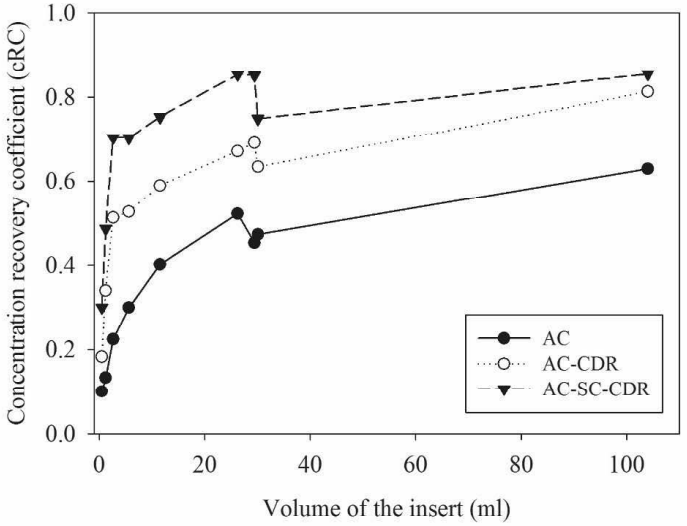

Figure 5-6. Quantification accuracy of ^{177}Lu using SPECT/CT. Figure represent cRC using three reconstruction compensation methods. Smaller volumes are less accurately quantified due to partial volume effect.

From patient data, higher activities were also measured from kidneys with AC-SC-CDR method than AC or AC-CDR methods. In Figure *5-7*, effective half-life estimates and calculated absorbed doses from patient data are shown using all three methods. AC-SC-CDR produced slightly shorter T_{eff} with smallest interpatient variation than other methods.

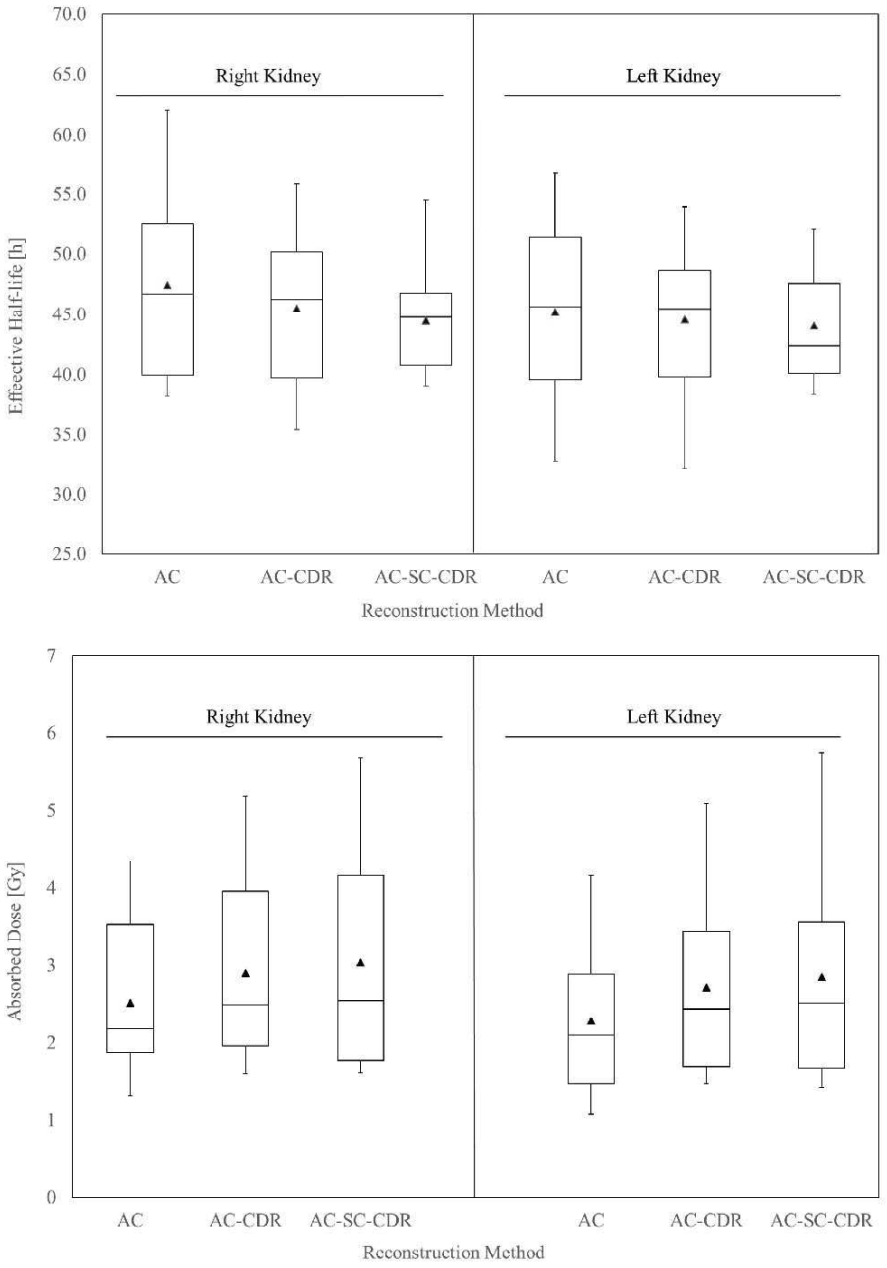

Figure 5-7 Box plots of effective half-life (above) and absorbed dose estimates (below) for right and left kidneys. The total number of patients was ten. The full triangles indicate mean values and the whiskers are extended to minimum and maximum data values (Spear style).

There was only one patient case, where AC method produced higher absorbed doses than other methods. This was due to the high uptake in liver metastases, which spills in to the right kidney volume in AC reconstruction, but which was reduced in AC-CDR and AC-SC-CDR reconstructions (Figure *5-8*)

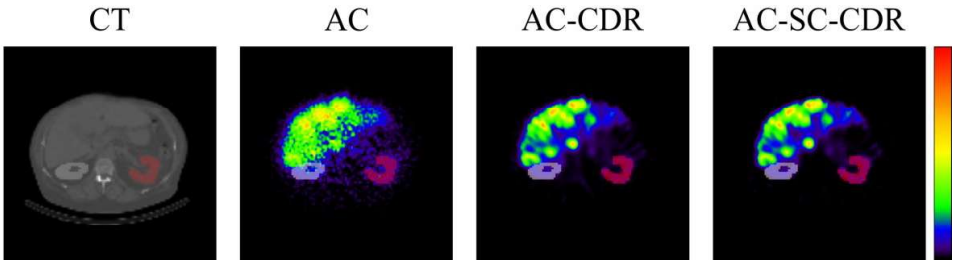

Figure 5-8. Transversal CT and SPECT slices of a patient case with numerous metastases in liver. Grey and red areas represent right and left kidney volumes. With AC-CDR or AC-SC-CDR compensations spill in from liver to right kidney volume was reduced.

5.2 Validation of sMC calculations method

Electrons emitted by ^{177}Lu can be assumed to absorb locally in voxel scales (~4 mm) that are currently used in SPECT imaging. This was shown in study **II** where absorbed dose produced by electrons was shown in DPK simulation to reduce down to 1% in the adjacent voxels compared to the source voxel. Using the ellipsoidal kidney models, the contribution of cross-irradiation to the target kidney was shown to be less than 1% when compared to the dose that kidney receives from self-irradiation, even when kidneys were touching each other (Figure *5-9*).

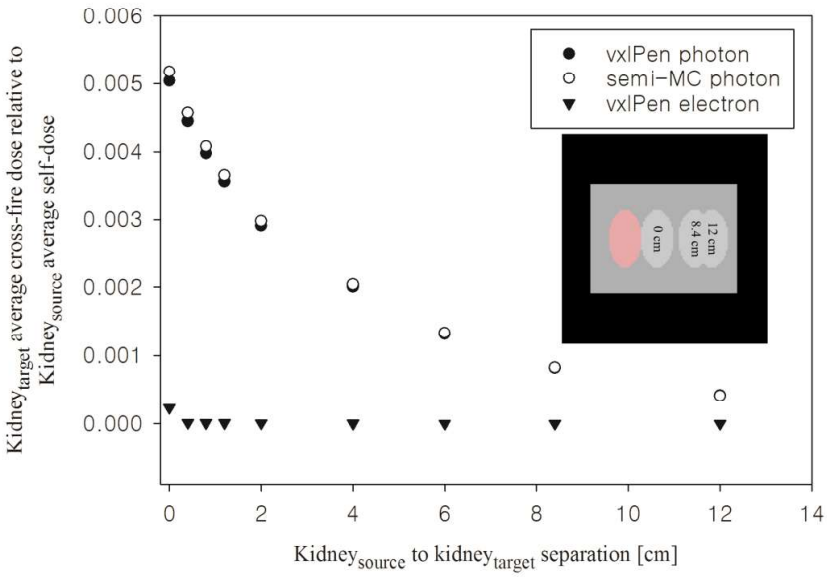

Figure 5-9. Cross-irradiation dose between source and target kidney models as function of distance. Cross-fire dose on y-axis is relative to self-irradiation dose of the target kidney. Photon doses were simulated using sMC (full circle) and vxlPen (circle) codes and electron doses (triangle) with vxlPen code.

On the other hand, when simulating a relatively high activity kidney model in semi-infinite soft tissue material, it was found that photons could produce a significant increase in dose heterogeneity on the surrounding voxels (Table 5-5). For example, 5% increase in absorbed dose was observed up to 5.8 cm (~14 voxels) range from the face of the model, when kidney to background concentration was 1:20. This could be significant in cases where highly active tumour or metastases are located next to the organ of interest, such as in a patient case in study **I** (Figure *5-8*).

Fast voxel-level absorbed dose calculation method sMC produced very similar average absorbed doses to kidneys when compared with detailed MC simulations (vxlPen). Comparison was done using simulated SPECT data in XCAT phantom geometry. The percentage differences between the methods were -0.4% and -5% for electron and photon doses, respectively, sMC producing smaller doses. Even the photon dose difference was clear as seen from dose rate volume histograms in Figure *5-10*, the average absorbed dose difference was -0.4% to both kidneys due to low emission abundance of photons.

Table 5-5. Relative increase in absorbed dose due to photon cross-fire for five different kidney to background concentration ratios.

Kidney to background activity ratio	From the kidney volume into the background: Distance from the kidney surface [cm]									From background into the kidney volume
	0.2	1.0	1.8	2.6	3.4	4.2	5.0	5.8	6.6	
1:1	1.02	1.01	1.01	1.01	1.00	1.00	1.00	1.00	1.00	1.1
2:1	1.03	1.02	1.01	1.01	1.01	1.01	1.01	1.00	1.00	1.05
5:1	1.08	1.06	1.04	1.03	1.02	1.02	1.01	1.01	1.01	1.02
10:1	1.17	1.11	1.07	1.06	1.04	1.04	1.03	1.02	1.02	1.01
20:1	1.34	1.23	1.15	1.11	1.09	1.07	1.06	1.05	1.04	1.01

The difference of the photon doses was further investigated by comparing electron and photon dose distribution separately using XCAT phantom. The biggest dose differences were observed in bone structures, which can partly be explained by the fact that sMC uses only water cross-sections for photon interaction modelling.

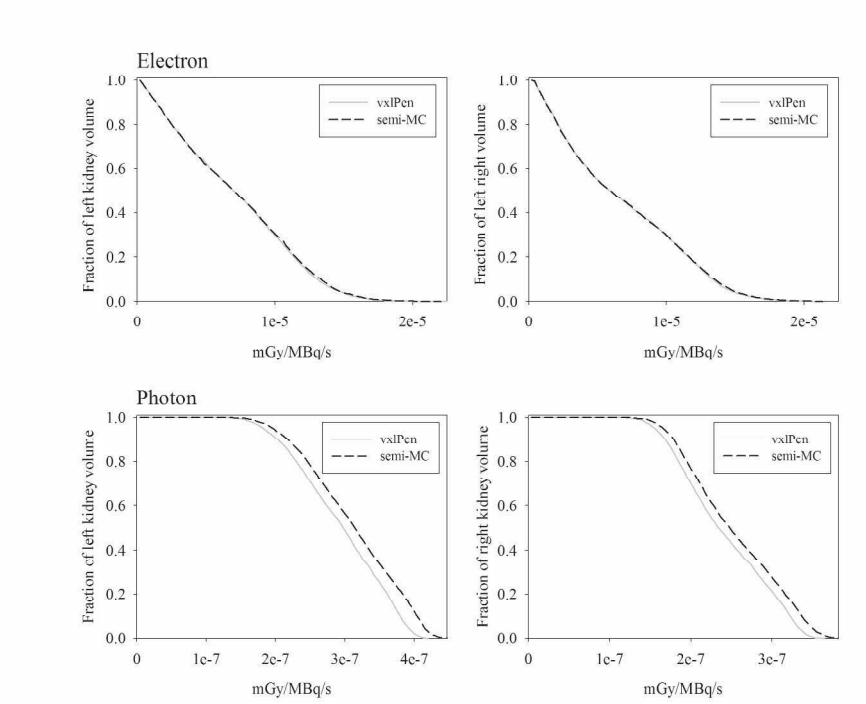

Figure 5-10. DrVHs of left and right kidneys of XCAT phantom simulated using vxlPen (solid line) and sMC (dashed line). The upper row shows electron dose distributions and the lower row shows photon dose distributions in kidney voxels.

5.3 Mean kidney doses in patients using OLINDA/EXM

Mean kidney dose and estimated maximum dose to kidneys were calculated using WKV and SV methods, respectively. A total of 96 treatments from 24 patients were analysed. The mean activity per treatment was 7.1 GBq for seventeen patients and the remaining seven patients, were treated with reduced activity due to clinical risk factors. The mean absorbed doses were 0.44 ± 0.15 Gy/GBq (range 0.22–1.05 Gy/GBq) and 0.74 ± 0.28 Gy/GBq (range 0.36–1.92 Gy/GBq) for WKV and SV methods, respectively. The difference between the methods was found to be significant ($p < 0.001$), which implies heterogeneity in kidney absorbed doses. Despite the absorbed dose difference between the methods, the effective half-life was estimated to be 45.3 ± 5.9 hours (range 35.5–58.9 hours) and 46.2 ± 5.6 hours (range 37.8–57.7 hours) using WKV and SV methods, respectively. The estimated absorbed doses and half-life times using WKV method are similar to those which were analysed in study **I** with HybridRecon and AC-SC-CDR compensation methods, where the mean absorbed dose was 0.44 Gy/GBq and T_{eff} was 44.3 hours from the subsample of 10 patients.

Kidney toxicity as measured by serum creatinine levels was not observed in any patient during the two year follow up after the treatment. On the other hand, grade I hematological toxicity was observed in 12 patients.

5.4 Voxel-level kidney dosimetry

Implementation of sMC method to HIRD was tested using simulated SPECT/CT data from XCAT phantom. The dosimetry package successfully reconstructed and calculated doses from simulated data. Analytically calculated $D_{ref,electron}$ (Equation 8) from the original TACs and simulated $D_{HIRD,electron}$ and $D_{HIRD,photon}$ doses are shown in Table 5-6. The difference between doses were within 6 % in all studied organs.

Table 5-6. *Comparison of electron absorbed doses between HIRD ($D_{HIRD,electron}$) and analytically calculated reference kidney doses ($D_{ref,electron}$). Photon contribution to organ doses calculated using HIRD is also shown ($D_{HIRD,photon}$).*

	Left Kidney	Right Kidney	Spleen	Tumour
$D_{ref,electron}$	9.42	9.42	16.39	20.84
$D_{HIRD,electron}$	10.01	9.85	16.34	21.15
Difference $(D_{HIRD,electron}-D_{ref})/D_{ref}$ (%)	6%	5%	0%	2%
$D_{HIRD,photon}$	0.56	0.49	0.67	0.67
$D_{HIRD,photon}$ / $D_{HIRD,Total}$ (%)	5%	5%	4%	3%

Patient kidney doses calculated with HIRD and OLINDA/EXM were compared using a relative Bland-Altman plot (Figure *5-11*). The mean difference between doses was 2%, the OLINDA/EXM producing slightly higher average doses. However, HIRD produces higher doses at doses below 2 Gy. This can be partly explained by photon cross-irradiation dose that is taken into account in the voxel level dose calculations by HIRD and photon cross-irradiation from high uptake volumes (e.g. metastases) in vicinity of the kidneys.

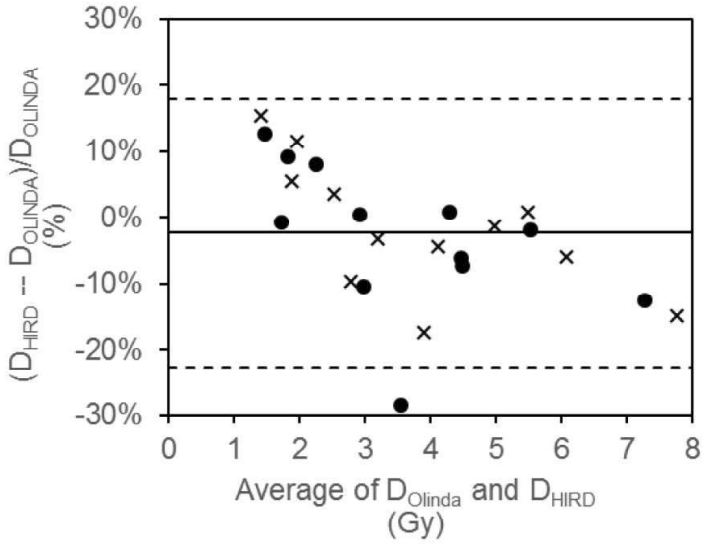

Figure 5-11. A relative Bland-Altman plot of kidney doses of OLINDA/EXM and HIRD. Doses to left (dot) and right (cross) kidneys are shown separately. The limits of agreement (dashed line), from -1.96SD to +1.96SD, were calculated for both kidneys together.

Photon dose contribution from high ^{177}Lu-DOTATATE tumour uptake was studied from a small number of patient cases. Figure *5-12* shows an example coronal CT image of a patient with relative low average kidney uptake but with high activity uptake in metastases next to the left kidney. The photon dose to left and right kidneys was 0.3 Gy (15% of total absorbed dose) and 0.2 Gy (9%), respectively. Part of the left kidney receives significantly higher doses (> 1 Gy) from photon cross-irradiation (Figure *5-12*, below).

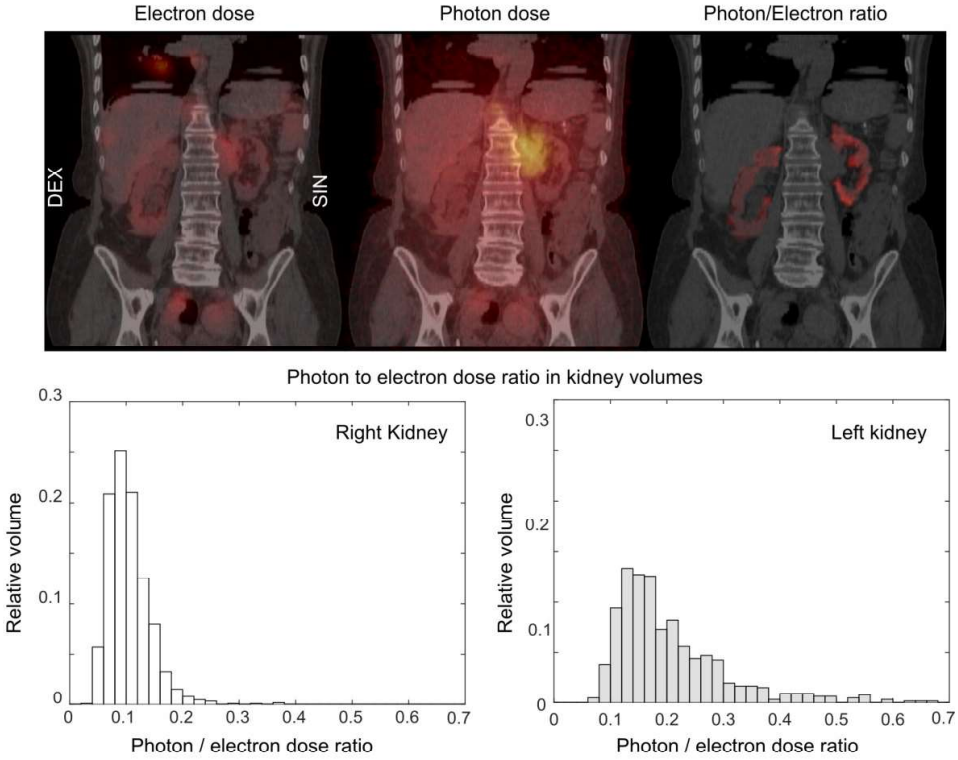

Figure 5-12. (Top) Coronal CT slices fused with electron and photon dose distributions from a patient case with a tumour mass next to left kidney. Ratio between photon and electron doses in kidney volumes is also visualised. (Below) Voxel level photon / electron dose ratio histograms from kidney volumes.

6 Discussion

In this thesis, radionuclide dosimetry methods were studied and voxel-level dosimetry software for radionuclide therapy was presented and validated. for kidney dosimetry after ^{177}Lu-DOTATATE treatment. Results of the original articles, included in this thesis, are discussed in more details in the corresponding papers. In this section, uncertainties in radionuclide dosimetry and other observations during software development are discussed. Discussion is concluded with future aspects of software development and implementations.

6.1 Determinants of SPECT image based dosimetry accuracy

SPECT image based dosimetry consists of five crucial steps, which are SPECT acquisition, quantitative image reconstruction, TAC analysis and integration, absorbed dose calculations and result analysis. Each of these steps can be dealt with separately, but in this thesis the last four steps were combined together to form a streamlined dosimetry software. The SPECT acquisition protocol used in this thesis was adopted from HUCH Comprehensive Cancer Center, where it was in used in clinical practice. Optimisation of acquisition protocol could have an impact on dosimetry accuracy, but due to practical reasons it was less emphasised in this thesis.

There are a number of potential sources of bias and variance in determining absolute activities using SPECT imaging. After injection, the kinetics of the injected radiopharmaceutical is followed with a series of SPECT/CT acquisitions. Depending on kinetics of the pharmaceutical in question, acquisitions can extend over a week. From acquired sinograms, three dimensional activity distributions are reconstructed and activity is quantified. In study **I**, the quantification accuracy of different reconstruction compensation methods, measured with cRC, was found to be of 0.85 for spherical ^{177}Lu sources with volumes larger than 25 ml (corresponding to a sphere with radius of 1.8 cm). For smaller sources quantification cannot be considered to be very reliable (Figure *5-6*). Similar results have been reported also by other authors [44, 46, 66-68]. It is known that CDR compensation method enhances so called Gibbs ringing artefacts in reconstructed images [69]. Even though the CDR improves quantification, for voxel level dosimetry this can be problematic, because the artefact distorts activity distribution, which can lead to false absorbed dose distributions. An example of the ringing artefact can be seen in Figure *4-3*, but it was however not observed in patient images (Figures *5-8* and *5-12*). There have been efforts to reduce the effect of the artefact [70], but further studies are needed to quantify its effect to absorbed dose calculations using clinical data.

Most of the quantification accuracy studies have been done using phantoms, which lacks the reality of clinical patient cases. However, *Sanders et al*. estimated urine activity concentration from SPECT/CT images and compared the results with urine samples measured with a well counter [67]. They reported a mean error of 10.1 ± 8.3% for

SPECT/CT concentration estimates. These kind of measurements give realistic understanding of the quantification accuracy of SPECT/CT methods and would have improved this thesis also.

The poor quantification accuracy of SPECT is mostly due to poor spatial and energy resolution of the gamma camera and this can be considered one of the limiting factors of SPECT image based quantification, and thus reliable dosimetry, especially for small organs or tumours. It should be noted that currently other clinically available imaging methods for therapeutic radiopharmaceuticals are not available, with the exception of PET for ^{90}Y.

Quantification accuracy is dependent on how imaging data is processed. As shown in Study **I**, compensation methods for confounding effects are important to improve quantification accuracy. However, iterative reconstruction is non-linear and has multiple parameters, which makes them more complex than analytical methods. Despite the complexity, iterative reconstruction algorithms are essential for quantitative SPECT imaging, because contrary to PET, SPECT attenuation correction has to be done during reconstruction and currently iterative methods are the only option for that. Due to complexity of iterative algorithms, the optimization of reconstruction parameters is laborious and an optimisation end point is hard to define. Simply put, reconstruction parameter optimisation is a trade-off between noise and quantification accuracy. In addition to parameters, variance in quantification is also dependent on the size of the source and the detected counts in raw projection data. For example, *Cheng et al.* optimised reconstruction parameters to improve DVH estimates using simulated data and they presented fifteen different iteration and filtering combinations for three studied organs (liver, kidney and renal cortices) at five different time points after injection [71]. Reconstruction parameters (number of iterations and subsets) used in this thesis was a compromise between reconstruction time, quantification accuracy and image noise. Organ of interest, kidney, was also taken into consideration. Selection was based on multiple phantom measurements and thousands of image reconstructions carried out prior to this thesis (data not published).

In addition to quantitative image reconstruction, image post-processing is also a major source of inaccuracy. Whether it is the determination of organ volume or activity in organ at different time points (TAC), defining the boundaries of region of interest produces substantial bias and variance to results. There are almost as many delineation methods as there are quantification or dosimetry studies. Mostly used methods are threshold or manual methods, although automatic segmentation methods have been utilised. Manual delineation is obviously very operator sensitive and prone to random errors. On the other hand, there is no correct threshold value for delineation, which is suitable for all SPECT data and source sizes, and thus the threshold method is also arbitrary. Despite several years of extensive research of the ideal delineation method for nuclear medicine images [72], the problem still remains unsolved. In this thesis, delineation was carried out manually along physical boundaries of the volume of interest with help from CT images (except the small volume method in study **III**). With organs like kidneys or phantoms,

manual delineation is usually relative easy to implement, though cumbersome in most cases. But in some cases where the region of interest is not visible in CT images, like tumours, manual delineation is impractical. The delineation based on physical boundaries from CT image has its disadvantages, the delineation rule is explicit and it also gives the volume (mass), which is needed for absorbed dose calculation.

Several studies have been carried out to solve the optimal number of SPECT acquisition time points for ^{177}Lu-DOTATATE treatments [43, 73-75]. Three to four time points over a week are considered to be adequate to sample TAC of simple kinetics of ^{177}Lu-DOTATATE in kidneys. Dosimetry protocols with several imaging visits to the hospital are burdensome for patients and for the nuclear medicine imaging facility. In study **III**, the fast kidney dose (FKD) protocol with two acquisition time-points was found to be adequate for estimation of mean absorbed dose to kidneys and the FDK protocol was implemented in clinical practice in HUCH Comprehensive Cancer Center. However, the kinetics of radiopharmaceuticals are rarely as simply as earlier presented. For example, ^{177}Lu-DOTATATE has been shown to have stable uptake even up to 20 hours in tumours [64]. The aim of this thesis was to perform absorbed dose calculations in voxel-level. Clinical SPECT images are noisy due to low statistics in acquired projection data and inherent properties of iterative reconstruction algorithms. Because of that, a mixed and restricted voxel level TIAC calculation method was implemented. In comparison study **IV**, the implemented voxel level dose calculation method was found to be feasible for kidneys and estimated doses were comparable with OLINDA/EXM calculation based on whole kidney volume activities and kinetics. However, for other organs and tumours further studies are needed to verify the present TIAC calculation method.

One part of this thesis was dedicated to absorbed dose calculations (study **II**). The study was designed to verify the fast sMC calculation method implemented in HIRD, and also to study photon cross-irradiation. Despite the relatively low abundance of photon emitted by ^{177}Lu, it was found that photons from high uptake volumes can produce significant dose heterogeneity in tissues around the source volume or cross-irradiation dose from several sources can accumulate to a relative high sum. This result is important for voxel-level dosimetry and examples of photon cross-irradiation was shown to be relevant in patients with low kidney uptake of ^{177}Lu-DOTATATE or with high uptake tumour masses in nearby organs (Figures *5-11* and *5-12*).

There are other factors which also affect the dose calculation accuracy, but their effect can be considered to be minor compared to the factors reviewed above. Physical properties of radionuclide and decay data scheme have their uncertainties, but they are many folds smaller than other factors discussed earlier. Nevertheless, implementation of decay data should be done carefully especially for radionuclides with a complex decay scheme.

6.2 Future aspects

Voxel-level dosimetry tools presented in this thesis can be implemented for other organs, radionuclides and imaging modalities than kidneys, ^{177}Lu and SPECT. One very interesting future research topic is tumour dosimetry and dose response of ^{177}Lu-DOTATATE, which is scarcely studied [19]. Another obvious topic is the implementation of dosimetry methods presented in this thesis for ^{177}Lu-PSMA treatments.

Using state-of-the-art reconstruction methods, voxel based dose analysis methods like dose volume histogram analysis could help to gain more insight into dose response and help to predict treatment outcomes. With the help of dose heterogeneity information, sophisticated radiobiological models could be used, which are a normal convention in external radiation treatments. This could also help to predict possible normal tissue complication and tumour responses.

In this thesis, all absorbed dose calculations were done after the patient received radionuclide therapy. Thus, dose calculations did not have a big predictive value, rather calculations were carried out for patient safety and legislation reasons and to follow up critical healthy tissue absorbed dose levels. In future, dosimetry needs also to be applied to predicted therapeutic response. DOTATATE can be radiolabelled with Gallium-68 (^{68}Ga) and then carry out the diagnostic imaging using PET. This gives possibilities to study radiopharmaceuticals kinetics before treatment and could help to choose patients who will benefit from the treatment. Due to the short half-life of ^{68}Ga, predicting the kinetics of DOTATATE from PET imaging is challenging, but a physiologically based pharmacokinetic (PBPK) model has been proposed to tackle this problem [76].

There are other dosimetry software packages available for radionuclide dosimetry (page 10, Table 2-1). As quantitative SPECT imaging and image based dosimetry become more common, one big step for the whole nuclear medicine community is to harmonize dosimetry methods so that calculated absorbed dose is equal globally. Similar efforts have been carried out for harmonising the standardised uptake value [77], which is a semi-quantitative measure used in diagnostic PET imaging. It would be important to carry out similar work for internal dosimetry too.

7 Conclusions

In this thesis, fundamental parts of radionuclide therapy dosimetry were studied and findings were used to develop voxel level dosimetry software for 177Lu-DOTATATE treatments. Software includes all the necessary steps from image reconstruction to absorbed dose calculations which streamlines daily practice. The voxel level dosimetry methodology was tested with phantoms and validated with patient data. The thesis reached its aims with the following main conclusions:

I An anthropomorphic phantom was used to show the importance of reconstruction compensation methods for ^{177}Lu activity quantification. Combining attenuation, Monte-Carlo scatter and collimator-detector-response compensation method dramatically improves quantification accuracy of small ^{177}Lu sources.

II For SPECT image based dosimetry with voxel size of 4 mm or higher, β^- radiation emitted by ^{177}Lu can be considered to be locally absorbed. On the other hand, cross-irradiation from gamma radiation can accumulate to relatively high absorbed dose levels or produce notable dose heterogeneity.

III Resident times of ^{177}Lu-DOTATATE measured from kidney using small volume or whole kidney region of interests does not significantly differ. However, small volume method is operator dependent. In addition, a small volume placed on the most active volume produced higher absorbed doses than whole kidney method. This implies heterogeneous activity accumulation and absorbed dose to kidneys.

IV Presented voxel level dosimetry software is feasible for kidney dosimetry of ^{177}Lu-DOTATATE treated patients. Software includes also cross-irradiation dose calculation from gamma emissions, which was shown to be relative high in some patient cases.

References

1. Välimäki, M.J. and J. Arola, *Ruoansulatuskanavan ja haiman neuroendokriiniset kasvaimet.* Duodecim, 2011. **127**(15): p. 1549-59.
2. Hallet, J., et al., *Exploring the rising incidence of neuroendocrine tumors: a population-based analysis of epidemiology, metastatic presentation, and outcomes.* Cancer, 2015. **121**(4): p. 589-97.
3. Modlin, I.M., et al., *Gastroenteropancreatic neuroendocrine tumours.* The Lancet Oncology, 2008. **9**(1): p. 61-72.
4. Oberg, K., et al., *Neuroendocrine gastro-entero-pancreatic tumors: ESMO Clinical Practice Guidelines for diagnosis, treatment and follow-up.* Ann Oncol, 2012. **23 Suppl 7**: p. vii124-30.
5. Kloppel, G., *Classification and pathology of gastroenteropancreatic neuroendocrine neoplasms.* Endocr Relat Cancer, 2011. **18 Suppl 1**(S1): p. S1-16.
6. Sorbye, H., et al., *Gastroenteropancreatic high-grade neuroendocrine carcinoma.* Cancer, 2014. **120**(18): p. 2814-23.
7. Korse, C.M., et al., *Incidence and survival of neuroendocrine tumours in the Netherlands according to histological grade: experience of two decades of cancer registry.* Eur J Cancer, 2013. **49**(8): p. 1975-83.
8. Bodei, L., et al., *Receptor radionuclide therapy with 90Y-[DOTA]0-Tyr3-octreotide (90Y-DOTATOC) in neuroendocrine tumours.* Eur J Nucl Med Mol Imaging, 2004. **31**(7): p. 1038-46.
9. Garkavij, M., et al., *177Lu-[DOTA0,Tyr3] octreotate therapy in patients with disseminated neuroendocrine tumors: Analysis of dosimetry with impact on future therapeutic strategy.* Cancer, 2010. **116**(4 Suppl): p. 1084-92.
10. Kwekkeboom, D.J., et al., *Treatment of patients with gastro-entero-pancreatic (GEP) tumours with the novel radiolabelled somatostatin analogue [177Lu-DOTA(0),Tyr3]octreotate.* Eur J Nucl Med Mol Imaging, 2003. **30**(3): p. 417-22.
11. Kwekkeboom, D.J., et al., *[177Lu-DOTAOTyr3]octreotate: comparison with [111In-DTPAo]octreotide in patients.* Eur J Nucl Med, 2001. **28**(9): p. 1319-25.
12. Kwekkeboom, D.J., et al., *Treatment with the radiolabeled somatostatin analog [177 Lu-DOTA 0,Tyr3]octreotate: toxicity, efficacy, and survival.* J Clin Oncol, 2008. **26**(13): p. 2124-30.
13. Strosberg, J., et al., *Phase 3 Trial of 177Lu-Dotatate for Midgut Neuroendocrine Tumors.* N Engl J Med, 2017. **376**(2): p. 125-135.
14. Strigari, L., et al., *The evidence base for the use of internal dosimetry in the clinical practice of molecular radiotherapy.* Eur J Nucl Med Mol Imaging, 2014. **41**(10): p. 1976-88.
15. O'Donoghue, J.A., et al., *Hematologic toxicity in radioimmunotherapy: dose-response relationships for I-131 labeled antibody therapy.* Cancer Biother Radiopharm, 2002. **17**(4): p. 435-43.
16. Breitz, H., et al., *Dosimetry of high dose skeletal targeted radiotherapy (STR) with 166Ho-DOTMP.* Cancer Biother Radiopharm, 2003. **18**(2): p. 225-30.
17. Bergsma, H., et al., *Nephrotoxicity after PRRT with (177)Lu-DOTA-octreotate.*

Eur J Nucl Med Mol Imaging, 2016. **43**(10): p. 1802-11.
18. Pauwels, S., et al., *Practical Dosimetry of Peptide Receptor Radionuclide Therapy with 90Y-Labeled Somatostatin Analogs.* Journal of Nuclear Medicine, 2005. **46**(1 suppl): p. 92S-98S.
19. Ilan, E., et al., *Dose response of pancreatic neuroendocrine tumors treated with peptide receptor radionuclide therapy using 177Lu-DOTATATE.* J Nucl Med, 2015. **56**(2): p. 177-82.
20. Zweit, J., *Radionuclides and carrier molecules for therapy.* Phys Med Biol, 1996. **41**(10): p. 1905-14.
21. Willowson, K., D.L. Bailey, and C. Baldock, *Quantitative SPECT reconstruction using CT-derived corrections.* Phys Med Biol, 2008. **53**(12): p. 3099-112.
22. Ritt, P., et al., *Absolute quantification in SPECT.* Eur J Nucl Med Mol Imaging, 2011. **38 Suppl 1**: p. S69-77.
23. Sandstrom, M., et al., *Individualized dosimetry in patients undergoing therapy with (177)Lu-DOTA-D-Phe (1)-Tyr (3)-octreotate.* Eur J Nucl Med Mol Imaging, 2010. **37**(2): p. 212-25.
24. Stabin, M.G., R.B. Sparks, and E. Crowe, *OLINDA/EXM: the second-generation personal computer software for internal dose assessment in nuclear medicine.* J Nucl Med, 2005. **46**(6): p. 1023-7.
25. Sgouros, G., *Dosimetry of internal emitters.* J Nucl Med, 2005. **46 Suppl 1**: p. 18S-27S.
26. Williams, L.E., G.L. DeNardo, and R.F. Meredith, *Targeted radionuclide therapy.* Medical Physics, 2008. **35**(7): p. 3062-3068.
27. Gleisner, K.S., et al., *Long-Term Retention of 177Lu/177mLu-DOTATATE in Patients Investigated by gamma-Spectrometry and gamma-Camera Imaging.* J Nucl Med, 2015. **56**(7): p. 976-84.
28. Dash, A., M.R. Pillai, and F.F. Knapp, Jr., *Production of (177)Lu for Targeted Radionuclide Therapy: Available Options.* Nucl Med Mol Imaging, 2015. **49**(2): p. 85-107.
29. Stabin, M.G. and L.C. da Luz, *Decay data for internal and external dose assessment.* Health Phys, 2002. **83**(4): p. 471-5.
30. Reijonen, V., et al., *Multicellular dosimetric chain for molecular radiotherapy exemplified with dose simulations on 3D cell spheroids.* Phys Med, 2017. **40**: p. 72-78.
31. Bé M.-M., et al., *Table of Radionuclides*. Monographie BIPM-5. Vol. 2. 2004, Pavillon de Breteuil, F-92310 Sévres, France: Bureau International des Poids et Mesures.
32. Dash, A., et al., *Peptide receptor radionuclide therapy: an overview.* Cancer Biother Radiopharm, 2015. **30**(2): p. 47-71.
33. de Jong, M., et al., *Comparison of (111)In-labeled somatostatin analogues for tumor scintigraphy and radionuclide therapy.* Cancer Res, 1998. **58**(3): p. 437-41.
34. Montgomery, W.W., *Surgery for acoustic neurinoma.* Ann Otol Rhinol Laryngol, 1973. **82**(4): p. 428-44.
35. National Research Council, *Health Risks from Exposure to Low Levels of Ionizing*

Radiation: BEIR VII Phase 2. 2006, Washington, DC: The National Academies Press. 422.
36. Visser, E., et al., *Software package for integrated data processing for internal dose assessment in nuclear medicine (SPRIND).* Eur J Nucl Med Mol Imaging, 2007. **34**(3): p. 413-21.
37. Glatting, G., et al., *Internal radionuclide therapy: the ULMDOS software for treatment planning.* Med Phys, 2005. **32**(7): p. 2399-405.
38. Divoli, A., et al., *Effect of patient morphology on dosimetric calculations for internal irradiation as assessed by comparisons of Monte Carlo versus conventional methodologies.* J Nucl Med, 2009. **50**(2): p. 316-23.
39. Ljungberg, M. and K. Sjogreen Gleisner, *Personalized Dosimetry for Radionuclide Therapy Using Molecular Imaging Tools.* Biomedicines, 2016. **4**(4): p. 25.
40. Grimes, J., C. Uribe, and A. Celler, *JADA: a graphical user interface for comprehensive internal dose assessment in nuclear medicine.* Med Phys, 2013. **40**(7): p. 072501.
41. He, B., et al., *Comparison of organ residence time estimation methods for radioimmunotherapy dosimetry and treatment planning--patient studies.* Med Phys, 2009. **36**(5): p. 1595-601.
42. He, B., et al., *Comparison of residence time estimation methods for radioimmunotherapy dosimetry and treatment planning--Monte Carlo simulation studies.* IEEE Trans Med Imaging, 2008. **27**(4): p. 521-30.
43. Sandstrom, M., et al., *Individualized dosimetry of kidney and bone marrow in patients undergoing 177Lu-DOTA-octreotate treatment.* J Nucl Med, 2013. **54**(1): p. 33-41.
44. Beauregard, J.M., et al., *Quantitative (177)Lu SPECT (QSPECT) imaging using a commercially available SPECT/CT system.* Cancer Imaging, 2011. **11**: p. 56-66.
45. Dewaraja, Y.K., et al., *MIRD pamphlet No. 23: quantitative SPECT for patient-specific 3-dimensional dosimetry in internal radionuclide therapy.* J Nucl Med, 2012. **53**(8): p. 1310-25.
46. de Nijs, R., et al., *Improving quantitative dosimetry in (177)Lu-DOTATATE SPECT by energy window-based scatter corrections.* Nucl Med Commun, 2014. **35**(5): p. 522-33.
47. Ljungberg, M., et al., *MIRD Pamphlet No. 26: Joint EANM/MIRD Guidelines for Quantitative 177Lu SPECT Applied for Dosimetry of Radiopharmaceutical Therapy.* J Nucl Med, 2016. **57**(1): p. 151-62.
48. Hudson, H.M. and R.S. Larkin, *Accelerated image reconstruction using ordered subsets of projection data.* IEEE Trans Med Imaging, 1994. **13**(4): p. 601-9.
49. Vija, A.H., E.G. Hawman, and J.C. Engdahl. *Analysis of a SPECT OSEM reconstruction method with 3D beam modeling and optional attenuation correction: phantom studies*. in *2003 IEEE Nuclear Science Symposium. Conference Record (IEEE Cat. No.03CH37515)*. 2003.
50. Sohlberg, A., H. Watabe, and H. Iida, *Three-dimensional SPECT reconstruction with transmission-dependent scatter correction.* Ann Nucl Med, 2008. **22**(7): p. 549-56.

51. Blankespoor, S.C., et al., *Attenuation correction of SPECT using X-ray CT on an emission-transmission CT system: Myocardial perfusion assessment.* 1995 Ieee Nuclear Science Symposium and Medical Imaging Conference Record, Vols 1-3, 1996: p. 1126-1130.
52. Tsui, B.M.W., et al., *Implementation of Simultaneous Attenuation and Detector Response Correction in Spect.* Ieee Transactions on Nuclear Science, 1988. **35**(1): p. 778-783.
53. Buvat, I., et al., *Scatter correction in scintigraphy: the state of the art.* Eur J Nucl Med, 1994. **21**(7): p. 675-94.
54. Ogawa, K., et al., *A practical method for position-dependent Compton-scatter correction in single photon emission CT.* IEEE Trans Med Imaging, 1991. **10**(3): p. 408-12.
55. Sohlberg, A., H. Watabe, and H. Iida, *Acceleration of Monte Carlo-based scatter compensation for cardiac SPECT.* Phys Med Biol, 2008. **53**(14): p. N277-85.
56. Kangasmaa, T.S., et al., *Multicenter evaluation of single-photon emission computed tomography quantification with third-party reconstruction software.* Nucl Med Commun, 2016. **37**(9): p. 983-7.
57. Bolch, W.E., et al., *MIRD pamphlet No. 21: a generalized schema for radiopharmaceutical dosimetry--standardization of nomenclature.* J Nucl Med, 2009. **50**(3): p. 477-84.
58. Woodcock, E., et al., *Techniques used in the GEM code for Monte Carlo neutronics calculation*, in *Proceedings of the Conference on Applications of Computing Methods to Reactor Problems*. 1965. p. 557.
59. Berger, M.J., et al., *XCOM: Photon Cross Section Database (version 1.5) [Online] Available: http://physics.nist.gov/xcom.* National Institute of Standards and Technology, Gaithersburg, MD, 2010: p. [Online] Available: http://physics.nist.gov/xcom.
60. Segars, W.P., et al., *4D XCAT phantom for multimodality imaging research.* Med Phys, 2010. **37**(9): p. 4902-15.
61. Sohlberg, A.O. and M.T. Kajaste, *Fast Monte Carlo-simulator with full collimator and detector response modelling for SPECT.* Ann Nucl Med, 2012. **26**(1): p. 92-8.
62. Bodei, L., et al., *The joint IAEA, EANM, and SNMMI practical guidance on peptide receptor radionuclide therapy (PRRNT) in neuroendocrine tumours.* Eur J Nucl Med Mol Imaging, 2013. **40**(5): p. 800-16.
63. Svensson, J., et al., *Renal function affects absorbed dose to the kidneys and haematological toxicity during (1)(7)(7)Lu-DOTATATE treatment.* Eur J Nucl Med Mol Imaging, 2015. **42**(6): p. 947-55.
64. Wehrmann, C., et al., *Results of individual patient dosimetry in peptide receptor radionuclide therapy with 177Lu DOTA-TATE and 177Lu DOTA-NOC.* Cancer Biother Radiopharm, 2007. **22**(3): p. 406-16.
65. Claringbold, P.G., et al., *Phase II study of radiopeptide 177Lu-octreotate and capecitabine therapy of progressive disseminated neuroendocrine tumours.* Eur J Nucl Med Mol Imaging, 2011. **38**(2): p. 302-11.
66. D'Arienzo, M., et al., *Quantitative 177Lu SPECT imaging using advanced*

correction algorithms in non-reference geometry. Phys Med, 2016. **32**(12): p. 1745-1752.
67. Sanders, J.C., et al., *Quantitative SPECT/CT Imaging of (177)Lu with In Vivo Validation in Patients Undergoing Peptide Receptor Radionuclide Therapy.* Mol Imaging Biol, 2015. **17**(4): p. 585-93.
68. Shcherbinin, S., et al., *Quantitative SPECT/CT reconstruction for (1)(7)(7)Lu and (1)(7)(7)Lu/(9)(0)Y targeted radionuclide therapies.* Phys Med Biol, 2012. **57**(18): p. 5733-47.
69. Farncombe, T.H., *Collimator-detector response compensation in quantitative SPECT reconstruction*, in *2007 IEEE Nuclear Science Symposium Conference Record*. 2007, IEEE. p. 3955-3960.
70. Kangasmaa, T., A. Sohlberg, and J.T. Kuikka, *Reduction of collimator correction artefacts with bayesian reconstruction in spect.* Int J Mol Imaging, 2011. **2011**: p. 630813.
71. Cheng, L., et al., *Improved dose-volume histogram estimates for radiopharmaceutical therapy by optimizing quantitative SPECT reconstruction parameters.* Phys Med Biol, 2013. **58**(11): p. 3631-47.
72. Fahey, F.H., et al., *Variability in PET quantitation within a multicenter consortium.* Med Phys, 2010. **37**(7): p. 3660-6.
73. Larsson, M., et al., *Estimation of absorbed dose to the kidneys in patients after treatment with 177Lu-octreotate: comparison between methods based on planar scintigraphy.* EJNMMI Res, 2012. **2**(1): p. 49.
74. Hanscheid, H., et al., *Dose Mapping after Endoradiotherapy with 177Lu-DOTATATE/-TOC by One Single Measurement after Four Days.* J Nucl Med, 2017.
75. Delker, A., et al., *The Influence of Early Measurements Onto the Estimated Kidney Dose in [(177)Lu][DOTA(0),Tyr(3)]Octreotate Peptide Receptor Radiotherapy of Neuroendocrine Tumors.* Mol Imaging Biol, 2015. **17**(5): p. 726-34.
76. Hardiansyah, D., et al., *Prediction of time-integrated activity coefficients in PRRT using simulated dynamic PET and a pharmacokinetic model.* Phys Med, 2017.
77. Boellaard, R., *Standards for PET image acquisition and quantitative data analysis.* J Nucl Med, 2009. **50 Suppl 1**: p. 11S-20S.